NASA TM-100515

NASA Technical Memorandum 100515

Preliminary 2-D Shell Analysis of the Space Shuttle Solid Rocket Boosters

Norman F. Knight, Jr., Ronnie E. Gillian and Michael P. Nemeth

March 1988

NASA
National Aeronautics and
Space Administration

Langley Research Center
Hampton, Virginia 23665

Preface

A two-dimensional shell model of an entire Solid Rocket Booster (SRB) has been developed using the STAGSC-1 computer code and preliminary 2-D shell analyses performed. The purpose of these analyses is to calculate the overall deflection distributions for the SRB when subjected to mechanical loads corresponding to critical times during the launch sequence. The mechanical loading conditions for the full SRB arise from the External Tank (ET) attachment points, the SRM pressure load, and the SRB hold down posts. The ET strut loads vary with time after the Space Shuttle Main Engine (SSME) ignition. The Solid Rocket Motor (SRM) internal pressure varies axially by approximately 100 psi. Static analyses of the full SRB are performed using a "snapshot picture" of the loads.

The SRB analyses are performed using various NASA computer systems. In building the finite element models, calculating results, and evaluating the output, three different classes of computer systems are used (i.e., workstations, minicomputers and supercomputers). A fourth class of computer system, the mainframe system, is used to store data, process microfiche, and produce report-quality graphics output. The computational approach using this variety of computer systems is described.

i

N88-23989 #

TABLE OF CONTENTS

PRELIMINARY 2-D SHELL ANALYSIS
OF THE SPACE SHUTTLE
SOLID ROCKET BOOSTERS

Norman F. Knight, Jr.[†], Ronnie E. Gilliam[‡], and Michael P. Nemeth[†]
NASA Langley Research Center
Hampton, Virginia

Introduction

The basic elements of the Space Shuttle system are the Orbiter, the External Tank (ET), and the two re-usable Solid Rocket Boosters (SRB's) as shown in figure 1. The SRB's provide the primary Shuttle ascent boost for the first two minutes of flight with an assist from the three Space Shuttle Main Engines (SSME's) on the Orbiter. The SRB structural subsystems are depicted in figure 2 and further described in reference 1. A major subsystem of the SRB is the Solid Rocket Motor (SRM) which consists of four lined, insulated rocket motor segments. These segments are connected using pinned tang-clevis joints. A cross section of a tang-clevis joint is shown in figure 3. The upper end of the lower cylindrical, motor segment forms the clevis. The lower end of the upper cylindrical, motor segment forms the tang which mates with the lower clevis. Around the circumference of both tang and clevis ends are 180 holes into which one-inch-diameter connecting pins are inserted. Three of the pin holes on the tang end are used as alignment slots to facilitate assembly of the SRM segments. The remaining 177 pins are load bearing and after assembly are held in place by retainer bands. The seal between two motor segments is provided by two O-rings in the "inner arm" of the clevis. The O-rings are compressed upon assembly of the SRM segments by a flat sealing surface on the tang.

The accident which destroyed the Space Shuttle Challenger is believed to have been caused by the failure of a case joint in the right solid rocket motor.[2] Several characteristics of the original SRM joint design have been identified as potential contributors to the failure. One characteristic is the behavior of the joint under internal pressure load. The motor case expands radially outward due to the pressure. Because the joint has a higher hoop

---

[†] Aerospace Engineers, Structural Mechanics Branch, Structures and Dynamics Division.
[‡] Mathematician, Structural Mechanics Branch, Structures and Dynamics Division.

stiffness than the case wall on either side of the joint, its radial expansion is less than that of the case wall. This nonuniform radial expansion is the primary cause of relative motion between the inner clevis arm and the sealing surface on the tang. This relative motion can cause the O-rings to become unseated and therefore lose their sealing capability.

Structural analyses at various levels of detail, as indicated on figure 4, have been performed in support of the SRB structural design assessment and redesign efforts. These levels vary from local three-dimensional solid models of a one-degree segment of the tang-clevis joint reported in reference 3 to global shell models of the entire SRB (four segment model) reported herein. Axisymmetric shell-of-revolution and axisymmetric solid models of the local joint have been analyzed wherein the overall shell response characteristics are represented well. However, the use of these models to determine the structural response locally in the joint requires substantial engineering judgement due to inherent asymmetries associated with the pins, friction, and contact. The three-dimensional solid models of a one-degree segment (centerline of a pin to midway between pins) of the field joint were used to determine the local joint response to pressure loading including the induced axial load. The four segment shell model of the entire SRB uses equivalent stiffness joint models and as such cannot predict the local joint behavior. A two-dimensional shell model of the right SRB has been developed using the STAGSC-1 computer code[4,5]. A representative STAGSC-1 input data case is given in Appendix A. This 2-D shell model has been used to calculate the overall deflection distributions for the SRB when subjected to mechanical loads corresponding to selected times during the launch sequence. The mechanical loading conditions for the full SRB arise from the ET attachment points, the SRM pressure load, and the SRB aft skirt hold down posts. The ET strut loads vary with time after SSME ignition. The SRM internal pressure varies axially by approximately 100 psi. Static analyses of the full SRB will be performed using a "snapshot picture" of the loads. The purpose of this paper is to document the SRB finite element model, to describe the computational approach and requirements, and to present results from preliminary analyses of the SRB subjected to selected pre-liftoff loads of STS 51-L.

Method of Analysis

The STAGSC-1 computer code[4,5] has been under development for over 15 years and its development was initiated to support the design and analysis of the space shuttle

2

system. The principal developers were Bo Almroth, Frank Brogan, Gary Stanley, and Charles Rankin of the Lockheed Palo Alto Research Laboratory. STAGSC-1 is a 2-D shell finite element analysis code based on the displacement formulation. The element library includes nonlinear spring or mount elements, 1-D beam elements, and 2-D plate/shell elements. Analysis options are provided for including geometric and material nonlinearities for buckling, collapse, vibration, or transient dynamic analysis. STAGSC-1 is supported on CDC, VAX, and Cray computers and is available through COSMIC.

The STAGSC-1 computer code is comprised of six modules: STAGS1; STAGS2; UNFFMT; FMTUNF; POSTP; and STAPL. The STAGS1 module is a preprocessing module which handles model generation, degree-of-freedom tables, element shape functions, element constitutive matrices, and so forth. Execution of this module typically precedes the execution of STAGS2, POSTP, or STAPL. The STAGS2 module is the computational module which performs matrix decomposition, linear and nonlinear stress analyses, eigenvalue (buckling or vibration) analyses, transient dynamic response predictions, and so forth. The modules UNFFMT and FMTUNF are used to translate the STAGS restart file (TAPE22) to an ASCII file for transfer to another computer type and then to convert that ASCII file back to a STAGS restart file for further processing. For example, the analysis could be performed on a Cray computer and the restart file translated into ASCII format. This ASCII file is transferred to a different computer system, say a VAX, and then converted back to a restart file for postprocessing. The POSTP module is a postprocessing module for printing primary solutions or recovering secondary solutions (such as stresses, strains, stress resultants) from previously calculated displacement solutions which have been written to the restart file. The STAPL module is also a postprocessing module for plotting undeformed and deformed geometries, as well as contour plots of solution vectors (primary or secondary solutions).

Finite Element Modeling

The modeling strategy used in the STAGSC-1 computer code involves the concepts of a shell unit and an element unit. A shell unit may be viewed as a substructure or superelement for the purpose of modeling convenience only. A shell unit may be composed of hundreds of nodes and elements, and automatic mesh generation facilities are provided for several common geometries for plate and shell structures. Mesh generation for a shell

3

unit is accomplished by specifying the number of rows and columns of grid lines in each coordinate direction, not the number of elements. For example, a mesh with two rows and two columns represents one quadrilateral finite element. An element unit is perhaps more like conventional finite element codes in terms of required input data (e.g., node and element numbers, nodal coordinates, nodal connectivities) and provides the flexibility to model general shell-type structures. User-written subroutines are available for the user to write mesh generation utilities that meet specific needs. For example, the user-written subroutine WALL given in Appendix B is used in the analyses reported herein to vary the shell wall properties longitudinally along the SRB.

The finite element model used in these analyses is shown in figure 5. The modeling philosophy adopted in this study was substantially influenced by the size of the structure to be analyzed and the resulting number of the degrees-of-freedom in the equations to be solved. The underlying philosophy was to construct a finite element model that would accurately reflect the global load transfer in the SRB in a manner such that nonlinear shell collapse and shell ovalization under pre-launch loads could be assessed. Although, the resulting finite element model involved nearly 85,000 degrees-of-freedom, it does not have the necessary fidelity to determine detailed stress distributions in particular SRB subsystems. The following sections briefly describe some of the particular details of the finite element modeling for the entire SRB shell structure.

SRB Overview

The SRB structural subsystem provides the necessary structural support for the Shuttle vehicle on the launch pad, transfers thrust loads to the Orbiter and ET, and provides the housing, structural support and bracketry needed for the recovery system, the electrical components, the separation motors, and the thrust vector control system. This subsystem consists of the nose cone assembly, the forward skirt including the forward SRB/ET attach fitting, the aft SRB/ET attach ring and attach struts, the aft skirt including the heat shield, the systems tunnel, and structure for mounting other SRB subsystems components. In addition to these subsystems, the SRB also contains the SRM.

Each SRB is approximately 144 feet long and 12 feet in diameter. The rocket consists of several segments that are located along its length by station numbers that correspond to the x-coordinate of the right SRB coordinate system (see figure 6). These segments are

4

the forward nose cone assembly (station 201.0 to 523.8), the forward motor case (station 485.4 to 851.48), the forward center motor case (station 851.48 to 1171.48), the aft center motor case (station 1171.48 to 1491.48), the aft attach motor case (station 1491.48 to 1823.85), and the aft skirt and nozzle assembly (station 1823.85 to 1931.18). The motor cases connected together by a tang-clevis joint are assembled at the launch site. These joints are referred to as "field joints". Field joints are located at stations 851.48, 1171.48, and 1491.48. Each of the upper three motor segments contain an additional tang-clevis joint that is assembled at the factory. These joints are referred to as "factory joints". The aft attach motor case has two of these factory joints. In addition, the forward motor case and the aft attach case each have what is referred to as a "Y-shaped factory joint" that connects the pressure domes to the SRM. These Y-shaped factory joints have an appendage that is used to connect the forward nose assembly and the aft skirt to the SRM.

Equivalent Joint Modeling

The factory and field joints of the SRB are complicated structural assemblies that behave nonlinearly due to contact, friction, and local material yielding in the joints. In the present analysis, the field and factory joints are modeled by using equivalent stiffness joints as indicated in figure 7 instead of detailed models of the joint. As such, the influence of the joints on the global shell response is included; however, local joint behavior (i.e., gap motion) cannot be recovered from these global models. Local structural behavior of the joints is described in detail in reference 3. Global shell behavior of the SRB can be obtained using equivalent stiffness joints for the field and factor joints, and an evaluation of nonlinear effects such as shell collapse and ovalization can be performed.

In keeping with the underlying modeling philosophy of the SRB shell structure, the assembly joints of the SRB were modeled by 2-D shell elements that were assigned stiffnesses that reflected the membrane, bending, and shear load transfer through the joints in a statically-equivalent manner. The properties for the equivalent stiffness joint are determined through parametric studies and comparisons with the referee test data[6]. In these studies, the SRM shell wall thickness was varied in the vicinity of the joints as indicated in figure 7. When a combination of thickness and effective length for the joints yields analytical results which agree with the measured radial deflections from the referee test girth gages, the equivalent stiffness joint properties are determined. In these analyses, the

5

equivalent joint is modeled as a 6-inch-long portion of the shell with an 0.8-inch thickness.

SRB Component Geometry and Modeling

Forward Cone.- The forward cone includes a nose cap and a frustrum. The nose cap is basically an aluminum monocoque structure with a hemispherical section at the forward end. The base is approximately 68 inches in diameter and has an overall length of 75 inches. This structure is a riveted assembly consisting of machined 2024 aluminum sheet skins, formed ring segments, machined fittings, a formed cap, and a machined separation ring. The nose cap houses both the pilot and drogue parachutes. The frustum assembly is composed of machined 2210 aluminum shear beams, rings, fittings, separation motor supports, main parachute supports, and 7075 aluminum formed skins. The frustum is approximately 120 inches in height and has major and minor base diameters of 146 inches and 68 inches, respectively. The frustum houses the main parachutes, the altitude sensor, the forward separation motors, and incorporates flotation devices for water recovery.

The finite element model of the forward cone is shown in figure 8 and defined as shell unit 1 in the STAGSC-1 model listed in Appendix A . The forward cone is approximated by a conical surface with a height of 195.0 inches and a base radius of 72.62 inches. The shell thickness of this unit is considered to be uniform and has a value of 0.5 inches. During the time the 2-D shell model was being developed and analyzed, limited detailed information on the SRB was available — partly due to the accident investigation. Thus, certain assumptions had to be made for some SRB components in order to proceed with these studies. One such assumption is that the material properties for the forward cone are those of steel instead of aluminum. Since the forward cone is not subjected to any direct mechanical loads (e.g., internal pressure or SRB/ET interface loads), this assumption should have minimal affect on the overall shell response. The discretization involves 45 elements around the shell circumference and 10 elements longitudinally. No stringers or rings are included in the model of this component.

Forward Skirt.- The forward skirt comprises all structure between the forward SRM segment and the nose cone assembly. The forward skirt is cylindrical in shape, approximately 123 inches long, 146 inches in diameter, and is fabricated from 2219 aluminum. It includes the forward SRB/ET attachment fitting shown in figure 9 which transfers the thrust loads to the ET and a forward bulkhead which seals the forward end of the skirt.

The forward SRB/ET attachment fitting is a momentless joint that provides load transfer capability in the X-, Y-, and Z-directions as shown in figure 9 (i.e., SRB/ET interface load components denoted as P14, P15, and P16). The forward skirt provides the necessary structure to react the parachute loads during deployment and descent and a towing pendant assembly utilized during retrieval operations.

The finite element model of the forward skirt is shown in figure 10 and defined as shell unit 2 in the STAGSC-1 model listed in Appendix A. The cylindrical surface has a 72.62-inch radius and has an overall length of 135.48 inches. The shell thickness is uniform over the first 132.48 inches with a thickness of 0.5 inches. The last three inches of the model represent part of an equivalent joint. The discretization of the forward skirt involves 45 elements around the shell circumference and a total of 10 elements longitudinally. The discretization along the length varies to locate the forward ET ring and the joint. The forward ET ring is modeled as three discrete rings which are located at the third, fourth, and fifth longitudinal grid lines to insure a smooth load introduction in the model.

Aft Cylinder Skirt.- The finite element model of the aft cylinder skirt is shown in figure 11 and defined as shell unit 14 in the STAGSC-1 model listed in Appendix A. The cylindrical surface has a 72.62-inch radius and has an overall length of 13.24 inches. The shell thickness is uniform with a thickness of 0.5 inches. The discretization of the aft cylinder skirt involves 45 elements around the shell circumference and a total of 2 elements longitudinally. The discretization along the length varies to locate the kick ring. The kick ring shown on figure 12 provides the necessary structural capability to absorb and transfer induced prelaunch loads. The kick ring which bolts to the aft skirt is machined D6AC steel. The kick ring is modeled as two discrete rings which are located at the first and second longitudinal grid lines.

Aft Conical Skirt.- The aft conical skirt shown in figure 13 provides four attachment points (see figure 14) to the Mobile Launch Platform (MLP) and provides support to the Shuttle on the launch pad for all conditions prior to SRB ignition. The aft conical skirt also provides aerodynamic protection, thermal protection, and mounting provisions for the Thrust Vector Control (TVC) subsystem, and the aft mounted Booster Separation Motors (BSM). The aft conical skirt has a 146-inch minor diameter, a 212-inch major diameter, and a height of 90.5 inches. It consists of an integral stringer/skin construction that is welded and also has three bolted-on rings that are fabricated from 2219 aluminum.

7

The finite element model of the aft conical skirt is shown in figure 15 and defined as shell unit 15 in the STAGSC-1 model listed in Appendix A. The model of the aft skirt is 93.09 inches in height with a 208.2-inch major diameter and a 145.24-inch minor diameter. The finite element mesh for the aft skirt includes one element for the first 3.09 inches longitudinally and ten elements uniformly spaced over the remaining 90.0 inches. Forty-five elements are uniformly spaced around the shell. The shell thickness is assumed to be 0.5 inches. Twenty-four stringers spaced fifteen degrees apart are modeled as discrete beams. In addition, the three rings in the aft skirt are also modeled as discrete beams; however, their stiffness properties are distributed over two rings of nodes in the finite element model. The four hold down posts are each modeled as discrete beams with their stiffness properties distributed over two columns of nodes. These approximations are adequate for determining global shell behavior of the SRB. Detailed stress analysis of the aft skirt component would require substantially more modeling detail than is currently provided in this model.

ETA Ring Assembly.- The aft ETA ring assembly shown in figure 16 and its center is located at station 1511, approximately twenty inches below the aft attachment segment field joint. The ETA ring assembly is comprised of two tapered, partial rings(ring webs are approximately 12 inches apart), H-fittings to attach the ET struts, cover plates, and various other intercostals and brackets. The ETA rings are bolted every 2-degrees around the circumference to two stub rings which are integral parts of the SRM aft attachment segment. The ETA ring assembly extends only 270-degrees circumferentially around the SRM segment. Three struts attach the aft end of the SRB with the ET as shown in figure 17. These three attachment struts are designated the lower strut (P9), the diagonal strut (P10), and the upper strut (P8).

The finite element model of the ETA ring is shown in figure 18 and defined as an element unit in the STAGSC-1 model listed in Appendix A. User-written subroutine USRPT (see Appendix C) and USRELT (see Appendix D) are used to generate the geometry and finite element discretization of the ETA ring. The ETA ring webs are modeled with one element through the depth of the web and has a uniform thickness of 0.25 inches. The ETA ring cap is modeled as a discrete stiffener with a rectangular cross section of 1.0 inches by 1.79 inches. The ETA ring cover plates, intercostals, H-fittings, and various other brackets are not included in these finite element models. Further discussion of the SRB/ETA ring interface is provided in reference 7.

SRM Component Geometry and Modeling

The SRM case functions as a pressure vessel in which thrust can be developed, and as a structural frame through which flight loads are transmitted and reacted. The case construction is a D6AC steel forging with no welds forming each of 11 subassemblies as indicated on figure 19. These subassemblies are designated as the forward subassembly, six cylindrical subassemblies, the ET attachment subassembly, two stiffener subassemblies, and the aft subassembly. The eleven subassemblies are pre-assembled in four segments prior to propellant casting. These four segments are designated as the forward casting segment, two center casting segments (forward and aft), and the aft casting segment. These individual subassemblies are joined with pinned tang-clevis joints and pin retainer bands which hold the pins in place and also provide environmental seals for each joint (see figure 20). Attachment of the igniter and the nozzle is by means of polar bolt circles in the forward and aft subassemblies, respectively. The assembled SRM case has a nominal overall length of 1388 inches with a case thickness of 0.5 inches. These analyses did not distinguish between a standard SRM case and a lightweight HPM (high performance motor) case. The outside diameter of the basic cylindrical wall is 146 inches.

Forward Dome.- The forward dome caps the SRM as shown in figure 19. The finite element model of the forward dome is shown in figure 21 and defined as shell unit 3 in the STAGSC-1 model listed in Appendix A. The forward dome is modeled as a D6AC steel spherical segment with a radius of 81.25 inches, a subtended angle of 63.35 degrees, and a uniform thickness of 0.5 inches. Sixteen quadrilateral elements and a triangular element at the pole define one strip of elements along the meridian. Forty-five strips of elements are uniformly distributed around the shell. The forward dome is loaded by internal pressure which results in the axial load in the remaining SRM segments.

Forward Segment.- The forward segment includes two cylindrical cases (see figure 19) and has an overall length of 320 inches. The radius of the shell is 72.62 inches and, with the exception of the equivalent stiffness joints, the shell thickness is uniformly 0.5 inches thick. Tang-clevis joints are located at either end of the case and also at the center. The joints at the ends are field joints and the center joint is a factory joint. These names refer to location where the motor segment is assembled (i.e., at the factory or at the launch site). These joints are structurally identical; however, different SRM internal insulation patterns are present at each type of joint to facilitate field assembly.

The finite element model of the forward segment is shown in figure 22 and defined as shell unit 4 in the STAGSC-1 model listed in Appendix A. This model is 320 inches long and has a total of 34 elements longitudinally and 45 elements circumerferentially. The longitudinal distribution of elements varies to account for the presence of the tang-clevis joints. This model is loaded by the SRM internal pressure along its length.

Center Forward Segment.- The center forward segment shown in figure 19 is identical to the forward segment except its location in the overall SRM. The top of this segment mates with the bottom of the forward segment to form a field joint connection.

The finite element model of the center forward segment is shown in figure 23 and defined as shell unit 5 in the STAGSC-1 model listed in Appendix A. This model is 320 inches long and has a total of 34 elements longitudinally and 45 elements circumerferentially. The longitudinal distribution of elements varies to account for the presence of the tang-clevis joints. This model is loaded by the SRM internal pressure along its length.

Center Aft Segment.- The center aft segment shown in figure 19 is identical to the previous two segments. The top of this segment mates with the bottom of the center forward segment to form a field joint connection.

The finite element model of the center aft case is shown in figure 24 and defined as shell unit 6 in the STAGSC-1 model listed in Appendix A. This model is 320 inches long and has a total of 34 elements longitudinally and 45 elements circumerferentially. The longitudinal distribution of elements varies to account for the presence of the tang-clevis joints. This model is loaded by the SRM internal pressure along its length.

Aft Segment.- The aft segment shown in figure 19 is comprised of several components which make this segment unique and different from the previous segments. This SRM segment includes the SRB/ETA ring interface region, the aft attach case with external stiffeners for stability under water impact loads on splashdown, and the aft dome. The exit nozzle of the SRB has not been included in these analyses. The top of this segment is at station 1491, the field joint which is believed to have caused the Challenger disaster. Approximately 12 inches below the field joint is the first SRM stub ring, and the second SRM stub ring is 12 inches below the first ring. Three additional factory joints are also located in the aft segment at stations 1577, 1697, and 1812 as indicated on figure 6.

The finite element model of the aft segment is divided into seven shell units for convenience of model generation. The boundaries of the shell units were selected on the basis

of the location of the SRM stub rings. Namely, shell units are defined for the aft segment above, between, and below the SRM stub rings, for each SRM stub ring, for the aft attach case, and for the aft dome.

The finite element model of the aft segment above the SRM stub rings is shown in figure 25 and defined as shell unit 7 in the STAGSC-1 model listed in Appendix A. This model is 13.54 inches long and has only 2 elements longitudinally and 45 elements circumferentially. The longitudinal distribution of elements varies to account for the presence of the tang-clevis joint at station 1491. This model is loaded by the SRM internal pressure along its length.

The finite element model of the aft segment between the aft SRM stub rings is shown in figure 26 and defined as shell unit 8 in the STAGSC-1 model listed in Appendix A. This model is 11.97 inches long and has only 2 elements longitudinally and 45 elements circumerferentially. The shell wall thickness of this portion of the aft segment is 0.62 inches and the reference surface of the shell is eccentrically located from the middle surface of this portion of the model. This model is loaded by the SRM internal pressure along its length.

The connection between the SRM stub rings of the SRM aft segment to the ETA ring webs is treated as a conventional finite element connection between adjacent elements in a model. This assumption implies that the stub ring and the ETA ring are "welded" together or that these parts are "integrally machined". The finite element model of the SRM stub rings is shown in figure 27 and defined as shell units 9 and 10 in the STAGSC-1 model listed in Appendix A. These stub rings were modeled as annular plates with an inner radius of 72.62 inches and an outer radius of 74.2578 inches. The thickness of each stub is 0.4 inches.

The finite element model of the aft segment below the SRM stub rings is shown in figure 28 and defined as shell unit 11 in the STAGSC-1 model listed in Appendix A. This model is 60.49 inches long and has a total of 7 elements longitudinally and 45 elements circumerferentially. The longitudinal distribution of elements varies to account for the presence of a tang-clevis joint. This model is loaded by the SRM internal pressure along its length.

Aft Attach Case.- The finite element model of the aft attach case is shown in figure 29 and defined as shell unit 12 in the STAGSC-1 model listed in Appendix A. This model is

246.37 inches long and has a total of 30 elements longitudinally and 45 elements circumferentially. The longitudinal distribution of elements varies to account for the presence of the tang-clevis joints. Four external ring stiffeners are located on the aft attach case for stability during water impact at splashdown. These rings are loacted at stations 1613, 1657, 1733, and 1777. The first two are stub rings and the second two are T-shaped ring stiffeners. These rings are modeled as discrete rings using beam elements. This model is loaded by the SRM internal pressure along its length.

Aft Dome.- The finite element model of the aft dome is shown in figure 30 and defined as shell unit 13 in the STAGSC-1 model listed in Appendix A. The aft dome is modeled as a spherical shell segment with an opening at the pole. This opening represents the location of the exit nozzle attachment. The spherical shell segment has a radius of 72.62 inches, a subtended angle of 43.49 degrees from a horizontal plane, and a uniform thickness of 0.362 inches. Eleven quadrilateral elements define one strip of elements along the meridan, and 45 strips of elements are distributed uniformly around the shell. The aft dome is not loaded to account for the presence of the nozzle aasembly.

SRB Loading

SRM Pressure Loading

The SRM pressure loading results from the burning of the solid propellant. Only the SRM components of the SRB are directly loaded by the internal pressure distribution. SRM ignition occurs approximately 6.6 seconds after SSME ignition and require 600 milliseconds to reach full pressurization. The SRM longitudinal pressure distribution given in reference 8 is shown in figure 31 and can be seen to vary by approximately 100 psi over the length of the SRM. User-written subroutine UPRESS is used to model this pressure variation (see Appendix E). The internal pressure elongates the SRM case before liftoff and imparts a significant load on the forward SRB/ET attach point. The SRM axial tension loads from SRM ignition to SRB separation are the result of internal pressure, thrust, and inertial loads.

SRB/ET Interface Loads

The reconstructed flight loads for the Space Shuttle Challenger Flight 51-L were obtained from NASA Johnson Space Center (JSC) initially in the form of strip charts and

later in the form of data stored on a magnetic tape. The loads data consist of equivalent beam forces and moments and vehicle interface loads for the first ten seconds of the flight. The equivalent beam forces and moments are given at 19 locations along the SRB and include inertial effects. The interface loads include components of the loads in the forward and aft struts connecting the SRB to the external tank as shown in figure 32. A computer program was written to extract the interface loads from the JSC database, compute the SRB/ET strut loads, and print the desired data. The struts loads as a function of time for the right SRB are given in figures 33 to 38. The loading cases considered in these analyses correspond to t = 0, 5.3, 6.6, and 7.2 seconds after SSME ignition. The time-consistent SRB/ET interface loads for these four "snapshots" in time are given in table 1.

Computational Approach

The SRB analyses are performed using various NASA computer systems. The operational aspects of this procedure involving remote access to the Numerical Aerodynamic Simulator (or NAS)[9] facility at the NASA Ames Research Center are described on figure 39. A Langley VAX is used for model preparation and verification. The datasets are then networked to the NAS computers for execution. The output files and restart files are returned to a Langley VAX for postprocessing. The output files and plot vector files are networked to the Langley central computer system for printing, microfiche, plotting, and archival storage. For example, a nonlinear analysis of the SRB is performed on the NAS Cray-2 computer and a restart file containing calculated displacement solution vectors is generated. Then the restart file is translated into ASCII format and transferred using NASnet to a Langley VAX computer. This ASCII file is converted back to a restart file for postprocessing. The output file (5 to 50 megabytes in size) generated on NAS is also returned to Langley and then transferred using LARCNET to the central computer site for microfiche copies (7 to 25 microfiche). The postprocessing of these results and the model verification task are performed on a Langley VAX computer system instead of the Langley central site CYBER computers because of the large memory requirements.

Computer Systems

These analyses were performed over the two years following the Space Shuttle Challenger disaster and used a variety of computer systems during that period. During this two year period, an integrated distributed computer environment was constructed from a con-

glomeration of individual computers scattered across the three thousand miles separating the Langley and Ames Research Centers. It began with a dependence on vendor specific operating systems and communication protocols (i.e., VAX/VMS, Cray COS, DECnet), and matured to an environment dominated by open-system architectures (i.e., UNIX and TCP/IP). In the beginning, redundant capabilities were required to prevent system, communication, or operational problems from hampering the failure investigation. Although familiarity with working in a distributed environment along with the development of more robust systems reduced the dependency on redundant systems to an acceptable level, a key to working in a distributed environment is developing such redundant capabilities. It is especially difficult to isolate and correct problems in a complex networked environment dominated by single-point-of-failure components.

In building the finite element models, calculating results, and evaluating the output, three different classes of computer systems are used (i.e., workstations, minicomputers and supercomputers). A fourth class of computer system, the mainframe system, is used to store data, process microfiche, and produce report-quality graphics output.

The first class of computer system used in building and verifying the finite element models is a minicomputer. A VAX 11/785 minicomputer running the VMS operating system is used. Since the STAGSC-1 computer code is developed and enhanced under the VMS operating system, this computer system is a natural part of the overall computing environment. The VAX 11/785 allowed the finite element models to be generated, solutions using coarse grids to be computed, and "quick-look" graphics output to be evaluated prior to submitting large-scale analyses to the supercomputer.

The second class of computer system used to perform these analyses is a VAXstation II GPX workstation running the ULTRIX operating system. This computer system provides basic communication between the VAX/VMS DECnet environment of a minicomputer and the UNIX TCP/IP environment of a supercomputer. The workstation capability also provides the "quick-look" graphics display to verify the model generation and to evaluate results.

The third class of computer systems used is supercomputers. The computational portion of these analyses is performed on the NAS facility at the NASA Ames Research Center. The goals and objectives of the NAS require that the computer system hardware and software change. At the beginning of this project, the NAS computer environment

was in transition. Cray Research, Inc. had delivered the first commercial Cray-2 super-computer, and an interim Cray X-MP/12 was still on-site at Ames. Work at NAS began using the Cray X-MP/12 supercomputer running the COS operating system. This Cray X-MP/12 was made available for the initial phase of the work. When the initial phase of the work was completed, the Cray X-MP/12 was removed, and the STAGSC-1 code was ported to the Cray-2 to complete the preliminary analyses reported in this paper. Various upgrades occurred during the remainder of this activity as NAS transitioned through a Cray-2 running UNICOS 1.0, a Cray-2 running UNICOS 2.0, and finally to a Cray-2S running UNICOS 3.0.

The NAS Cray-2 supercomputer has four processors, each with a clock cycle time of 4.1 billionths of a second and a total memory size of 256 million 64-bit words. This Cray-2 is a supercomputer capable of over one hundred times the computational capability of a VAX 11/785. In addition, the Cray-2 is a native 64-bit wordsize machine, and roundoff problems that are a problem on 32-bit machines are eliminated. The STAGSC-1 computer code, designed nearly fifteen years ago, uses basic algorithms that provide out-of-core solution methods that also work well on the Cray-2. Even with 256 million words of main memory, the larger matrices could not be held in memory. This application program made use of 60 million words of main memory (e.g., blank common is dimensioned to 32 million words) to avoid excessive I/O and to fit execution runs into the normal processing queues eliminating the need for special priority. Auxiliary data storage requirements for these analyses is another concern. During the large SRB runs, a single temporary file requires in excess of 800 megabytes of storage. Hence, coordination or scheduling of these runs by the analyst is necessary to avoid exceeding the available auxiliary storage.

Finally, the fourth class of computer system is the mainframe system. The Langley Central Site mainframe environment, consisting of several CDC Cyber computers run-ning the NOS operating system, provided a capability for producing printed output, mass storage for the large output files produced on the supercomputer, archival output in the form of microfiche, and report quality graphics. This local capability provided the labor intensive functions required throughout the distributed environment and complements the other distributed capabilities required for this project.

The changes occurring in the field of computer networking represent probably the most dramatic changes affecting structural analysts over the period of this project. Networking removed the constraint of physical distance. Working remotely from the supercomputers used in the computational phase of this project presented a new set of problems that, once solved, resulted in a unique new capability for the structural analysts.

Although work for this project culminated in a very complex network environment, it began as a much smaller effort. The effort began with an in-house network consisting of an Ethernet environment connecting a number of MicroVAXes, VAXes, and PC's within a building through a fiber optic network to the mainframe CDC computers. The final configuration resulted in a global network that supports every major communication protocol and many gateways. The initial communication link with Ames utilized a MicroVAX supported on the Science and Physics Access Network (SPAN)[10]. Utilizing a Vitalink Bridge which connects computer systems at the Langley Research Center to the NAS computer systems at Ames, communication through a VMS VAX at Ames provided access to the Cray X-MP/12 at Ames using the DECnet protocol in combination with the VAX VMS Cray Station software. When the UNICOS Cray-2 became avaliable, a communication link using the TCP/IP protocol was established.

The network at Langley uses Ethernet within buildings and a fiber optic Pronet 10 token-passing ring network called LARCnet between Langley buildings. Initially the gateways between buildings would route only a Xerox XNS-based protocol developed at Langley. Connecting to one of the Ethernets is a Vitalink Bridge that would route both TCP/IP and DECnet to the NAS facility at Ames over a 256 kilobits per second satellite link. The evolution of this network over the course of the project followed the networks developing in industry over that time. Much of the communication was done manually at first. LARCnet was used to copy files to a computer in the building that contained the Vitalink Bridge, and DECnet used to cross the country to a staging computer at Ames, and then the Cray Station software on the Ames VMS VAX to complete the link. The steps would be reversed to bring data back to Langley. This communication path simplified over the course of the project to the network now in place. Workstations in many buildings are supported with routing gateways through the LARCnet fiber optic system, through a Pronet P4200 gateway connected to the Vitalink directly. The communication link with Ames has been

upgraded to a one megabit per second transfer rate (i.e., T1 link) and it was discovered that a land line is preferable to a satellite link for interactive use. The result is that the miles between Ames and Langley are no longer a problem; researchers can use the NAS system at Ames as if it were located at Langley. The Cray-2 appears to the structural analyst as if it were embedded in the local workstation he uses.

UNICOS Conversion

The STAGSC-1 code was converted from the Cray COS system to the UNICOS system used by the Cray-2. This effort involved the conversion of approximately 90,000 lines of FORTRAN code to use the new cft77 compiler for the Cray-2. It also involved the conversion of I/O routines written in the Cray assembly language, CAL, for the Cray X-MP to C for the UNIX-based Cray-2 (see ref. 11). This conversion began the day the cft77 compiler for the Cray-2 was delivered to Ames as pre-release system software. Working closely with the Cray analysts, several compiler errors were identified, isolated, and corrective work-around procedures developed. The major portion of the code was converted in a week's time with only a couple of problems requiring additional effort. Compiler optimization problems and problems with passing character variables between FORTRAN and C routines proved to be the most difficult problems to solve. Intermittent problems with the "o-raw" qualifier on the C open directive caused early results to be dependent on the overall Cray-2 system workload. The internal memory management techniques made the STAGSC-1 code relatively easy to convert to the Cray-2, and very efficient once it was ported.

Performance

The performance of the STAGSC-1 program on the Cray X-MP/12 and Cray-2 computer is shown in table 2. Much of the early work was done without the advantage of FORTRAN optimization from the Cray-2 UNICOS 1.0 compiler due to the newness of the compiler and the errors in the compiler optimization. The Cray-2 flowtrace capability was used to identify the routines that required the most CPU time and efforts were directed at optimizing those routines. When the FORTRAN compiler optimization had been completed, the Cray-2 still took twice as long as the Cray X-MP/12 to perform a linear stress analysis of the SRB finite element model described in this paper. With the use of the Cray-2 vector library routine "sdot", the run time was decreased by a factor

17

of two, achieving the same overall rate as the Cray X-MP/12. Increasing the amount of memory managed within the program itself also resulted in significant I/O savings. Since STAGSC-1 was designed on static memory machines, the program made use of blank common to provide out-of-core solutions. By controlling the amount of managed memory within the STAGSC-1 program (i.e., changing the size of the blank common), the I/O rate required for efficient execution could be balanced with the restrictions of the specific implementation of UNICOS job processing.

A comparison of the NAS Cray-2 performance with the other classes of computers used in this study is given in table 3. The problem solved in this case is a linear stress analysis of the baseline finite element model of the SRB/ETA ring interface (see ref. 7). The finite element model has approximately 12,000 active degrees-of-freedom with an average semi-bandwidth of 510 in the global stiffness matrix. This problem is selected for comparison since it is the largest reasonable problem that could be expected to run on the VAX 11/785 (CPU speed limitation) and CDC NOS machines (fixed memory limitation). The times presented in table 3 are in CPU seconds and demonstrate clearly why a supercomputer is needed for these calculations, and it justifies the time spent in applying vector optimization techniques. The complete nonlinear shell analysis of the SRB for a pre-liftoff loading case required a total of nearly 3900 CPU seconds on the Cray-2.

Results and Discussion

The purpose of the 2-D shell analyses of an entire SRB is to calculate the overall deflection distributions for the SRB when subjected to mechanical loads corresponding to critical times during the launch sequence. The field and factory joints are modeled by using equivalent stiffness joints instead of detailed models of the joint. As such, local joint behavior cannot be obtained from this global model. However, global shell behavior can be obtained and an assessment of nonlinear effects such as shell collapse and ovalization can be performed for selected times during the launch sequence. The loading cases considered in these analyses correspond to the loadings at t = 0, 5.3, 6.6, and 7.2 seconds after SSME ignition. These four loading cases are used to examine the extremes of the actual loading expected prior to liftoff. The time-consistent SRB/ET interface loads for these four points in time are given in table 1.

At t = 0, the loads induced into the SRB's are due to the eccentric weight of the

Orbiter and ET and also due to cryogenic shrinkage of the ET during fueling. The t = 0 load case is included to investigate the initial static configuration prior to the ignition of the SSME's. The SRB finite element model with exaggerated deflections from a nonlinear analysis for the t = 0 load case is shown in figure 40.

When the SSME's are ignited, an eccentric thrust of approximately 1,000,000 pounds is produced that causes the Space Shuttle to bend over to a maximum deflection (referred to as "max twang"). Maximum bending occurs at t = 5.3 seconds after SSME ignition. The SRB finite element model with exaggerated deflections from a nonlinear analysis for the t = 5.3 seconds load case is shown in figure 41. Although the structural response of the SRB to the "max twang" loads at t = 5.3 seconds exhibits large deflections, the overall response as characterized by the SRB tip deflection is nearly linear as indicated in figure 42. Good correlation is shown between the SRB on-pad deflections given in figure 43 and in reference 12 for liftoff and FRF (Flight Readiness Firing) and the SRB tip deflection calculated using the time-consistent loads for t = 5.3 seconds.

The SSME's reach full thrust approximately 6.6 seconds after their ignition. At t = 6.6 seconds, the SRB has rebounded, and the signal is issued to ignite the SRM propellant and to release the bolts in the hold-down post of the aft skirt (see figures 13 and 14). The SRB finite element model with exaggerated deflections from a nonlinear analysis for the t = 6.6 seconds load case is shown in figure 44. Comparing the deformed geometries given in figure 41 for the "max twang" condition with that given in figure 44 for the SRM ignition condition indicates that the SRB is rebounding to its original position.

After approximately another 600 milliseconds (i.e., t = 7.2 seconds), the pressure inside the SRB has built up to nearly 1000 psi. The effect of the variation of the internal pressure distribution along the length of the SRM shown in figure 31 on the structural response is minimal. Since the SRB is not restrained to the launch pad at this time, liftoff occurs. However, the finite element model of the SRB for this load case assumes that the entire edge of the aft skirt is clamped so that the structural response for the pressurized SRM could be analyzed with the head pressure on the forward dome also applied. The SRB finite element model with exaggerated deflections from a linear analysis for the t = 7.2 seconds load case is shown in figure 45. Comparing the deformed geometries given in figures 41 and 43 for the unpressurized SRM condition with that given in figure 45 for the pressurized SRM condition indicates that the SRM field and factory joints influence

the global structural response much like frames on an aircraft fuselage (i.e., "pressure pillowing").

The global structural response of the SRB to these four loading cases (time-consistent SRB/ET interface loads for t = 0, 5.3, 6.6, and 7.2 seconds after SSME ignition) is given in figure 46. These four loading cases are used to examine the extremes of the actual loading expected prior to liftoff. At t = 0, the SRB's deflect toward the Orbiter due to the eccentric weight of the Orbiter and ET. At t = 5.3 seconds after SSME ignition, the SRB's deflect to a maximum value due to the eccentric thrust of the SSME's. At t = 6.6 seconds after SSME ignition, the SSME's reach for thrust, the Space Shuttle system is rebounding to its vertical position, and the SRM's are ignited. At t = 7.2 seconds after SSME ignition, the SRM's reach maximum operating pressure and liftoff occurs. No evidence of nonlinear shell collapse was observed in these preliminary 2-D shell analyses of the SRB for the pre-liftoff loading cases considered.

Summary

This paper documents the modeling philosophy used in developing a finite element model of the SRB. Details of the modeling are presented for each SRB component along with a representative input dataset for the STAGSC-1 computer code. User-written subroutines with inline comments are also included for completeness in the appendices.

The SRB analyses reported in this paper utilized various NASA computer systems. In building the finite element models, calculating results, evaluating the output, generating report-quality graphics output, and providing archival storage of datasets and results, four different classes of computer systems are used (i.e., workstations, minicomputers, mainframes, and supercomputers). The computational approach using this variety of computer systems is described.

The results of these analyses represent a preliminary assessment of the overall structural response of the SRB to selected pre-liftoff loads for STS 51-L. The present analyses neglect the effects of the SRM propellant and any dynamics. The field and factory tang-clevis joints are modeled as equivalent stiffness joints, and bolted connections (e.g., ETA rings) are modeled as "welded" sections.

The overall structural response predicted by these analyses characterizes the global shell behavior of the SRB. Future analytical studies may incorporate more detailed mod-

eling in selected regions, may include the SRM propellant, and may consider the dynamic response. In addition, flight loading conditions such as "max Q" should be assessed, and the influence of initial geometric imperfections on the structural behavior of the SRB should be determined.

Appendix A: Representative STAGSC-1 Data Case

```
1 FULL STACK MODEL OF RIGHT SRB ---SRM53N--- $A-1 12/8/86 - CRAY 2
2 C
3 C EQUIVALENT SHELL MODEL OF FIELD AND FACTORY JOINTS
4 C MODEL GOES FROM FORWARD CONE TO THE AFT SKIRT
5 C VARIATION IN SHELL WALL PROPERTIES MODELED
6 C USING SUBROUTINE WALL TO PICK THE WALL TABLE
7 C NUMBER FROM THE K-CARDS
8 C
9 C VARIATION IN SRM PRESSURE MODELED THROUGH SUBROUTINE UPRESS
10 C
11 C NONLINEAR ANALYSIS AT FULL LOAD
12 C
13 C LOADS AT T=5.3 SECONDS
14 C
15 C HOLD DOWN POSTS ON AFT SKIRT
16 C
17 C ASYMMETRIC ET FLANGES MODELED AS ELEMENT UNIT USING
18 C SUBROUTINES USRPT AND USRELT
19 C
20 3   1   1   0   0   0   1   0   $B-1
21 15   1   5   29   $B-2
22 3   9   14  1  $B-3
23 1.0   1.0   1.0   $C-1   LOAD FACTORS
24 0   9000   10   10   0     $D-1   SOLUTION STRATEGY
25 C
26 C MESH DISCRETIZATION
27 C
28 11 46,   $F-1   FORWARD CONE UNIT 1
29 11 46,   $F-1   FORWARD SKIRT UNIT 2
30 18 46,   $F-1   FORWARD DOME UNIT 3
31 35 46,   $F-1   FORWARD CASE UNIT 4
32 35 46,   $F-1   FORWARD CENTER CASE UNIT 5
33 35 46,   $F-1   AFT CENTER CASE UNIT 6
34  3 46,   $F-1   SEGMENT ABOVE AFT ET RINGS UNIT 7
35  3 46,   $F-1   SEGMENT BETWEEN AFT ET RINGS UNIT 8
36  2 46,   $F-1   UPPER AFT ET STUB RING UNIT 9
37  2 46,   $F-1   LOWER AFT ET STUB RING UNIT 10
38  8 46,   $F-1   SEGMENT BELOW AFT ET RINGS UNIT 11
39 31 46,   $F-1   AFT ATTACH CASE UNIT 12
40 10 46,   $F-1   AFT DOME UNIT 13
41  3 46,   $F-1   AFT SKIRT CYLINDER UNIT 14
42 12 46    $F-1   AFT SKIRT CONE UNIT 15
43 C
44 C FORWARD ET/SRB ATTACHMENT RING, AFT ET/SRB FLANGE CAPS,
45 C 2 STUB RINGS AND 2 T-SHAPED SPLASH DOWN RING STIFFENERS
46 C AFT CONICAL SKIRT RINGS AND STRINGERS
47 C _
48  2   3   0      $F-2 FWD ET/SRB LOAD INTRO RING
49 12   4   0      $F-2 AFT ATTACH CASE STUBS AND T RINGS
50 13   2   0      $F-2 AFT DOME BOSS RING
51 14   2   0      $F-2 AFT KICK RING
52 15   8   32     $F-2 AFT CONICAL SKIRT 4 RINGS 28 STRINGERS
53 C
54 C SHELL UNIT CONNECTION AND CLOSURE CARDS
55 C
56 1   2   1   4   $G-1 FWD CONE CLOSURE
57 1   3   2   1   $G-1
58 2   2   2   4   $G-1 FWD SKIRT CLOSURE
59 2   3   3   3   $G-1
60 2   3   4   1   $G-1
61 3   2   3   4   $G-1 FWD DOME CLOSURE
```

```
62 4  2  4   4   $G-1 FWD CASE CLOSURE
63 4  3  5   1   $G-1
64 5  2  5   4   $G-1 FWD CENTER CASE CLOSURE
65 5  3  6   1   $G-1
66 6  2  6   4   $G-1 AFT CENTER CASE CLOSURE
67 6  3  7   1   $G-1
68 7  2  7   4   $G-1 SEGMENT ABOVE AFT ET STUBS CLOSURE
69 7  3  8   1   $G-1
70 7  3  9   1   $G-1
71 8  2  8   4   $G-1 SEGMENT BETWEEN AFT ET STUBS CLOSURE
72 8  3  10  1   $G-1
73 8  3  11  1   $G-1
74 9  2  9   4   $G-1 UPPER AFT ET STUB CLOSURE
75 10 2  10  4   $G-1 LOWER AFT ET STUB CLOSURE
76 11 2  11  4   $G-1 SEGMENT BELOW AFT ET STUBS CLOSURE
77 11 3  12  1   $G-1
78 12 2  12  4   $G-1 AFT ATTACH CASE CLOSURE
79 12 3  13  1   $G-1
80 12 3  14  1   $G-1
81 13 2  13  4   $G-1 AFT DOME CLOSURE
82 14 2  14  4   $G-1 AFT SKIRT CYLINDER CLOSURE
83 14 3  15  1   $G-1
84 15 2  15  4   $G-1 AFT SKIRT CONE CLOSURE
85 C
86 C USER WRITTEN ROUTINES FOR USRELT,USRPT, AND WALL
87 C
88 0  0  0  0  0  1  1 $H-1
89 C
90 C D6AC STEEL PROPERTIES
91 C
92 1  $I-1
93 30.0E+6  0.3  0.0  0.283  $I-2
94 C
95 C ALUMINIUM PROPERTIES
96 C
97 2  $I-2
98 10.0E+6 0.3  0.0  0.102  $I-2
99 C
100 C DUMMY MATERIAL PROPERTIES
101 C
102 3  $I-2
103 0.1E+6 0.0  0.0  0.102  $I-2
104 C
105 C TABLE OF RING AND STRINGER PROPERTIES FOLLOWS
106 C
107 C
108 C FWD ET/SRB LOAD INTRO RING
109 C
110 1  1  1  0  2000.  0.  0.$J-1
111 10.  1000.  1000.  0.$J-2A
112 C
113 C ET FLANGE BOLT-ON RING CAPS
114 C
115 2  1  1  0  1.91178  0.0  0.0  $J-1
116 1.79  0.477945  0.149167  0.0  $J-2A
117 C
118 C STUB RINGS
119 C
120 3  1  1  0  0.0542  0.0  0.0  $J-1
121 0.34  0.0524  0.0018  0.0  $J-2A
122 C
123 C T-SHAPED RING PROPERTIES
124 C
125 4  1  1  0  3.5551  0.0  0.0  $J-1
```

```
126 1.5298  2.8355  0.7196  0.0  $J-2A
127 C
128 C AFT DOME BOSS RING
129 C
130 5  1  1  0  9.5319  0.0  0.0  $J-1
131 7.5625  4.766  4.766  0.0  $J-2A
132 C
133 C AFT CONICAL SKIRT RINGS
134 C
135 6  1  2  0  2000.  0.  0.$J-1
136 10.  1000.  1000.  0.$J-2A
137 C
138 C AFT CONICAL SKIRT STRINGERS
139 C
140 7  1  2  0  .0521  0.  0.$J-1
141 .5  .0417  .0104  0.$J-2A
142 C
143 C AFT HOLD-DOWN POSTS
144 C
145 8  1  2  0  2000.  0.  0.$J-1
146 10.  1000.  1000.  0.$J-2A
147 C
148 C FWD ET/SRB LOAD INTRO SIDE RINGS
149 C
150 9  1  3  0  2000.  0.  0.$J-1
151 10.  1000.  1000.  0.$J-2A
152 C
153 C SHELL WALL DEFINITIONS
154 C
155 1  1  1  $K-1 FORWARD CONE
156 2  0.5  $K-2
157 2  1  1  $K-1  FORWARD SKIRT
158 2  0.5  $K-2
159 3  1  1  $K-1 FORWARD DOME
160 1  0.5  $K-2
161 4  1  1  $K-1  FORWARD CASE
162 1  0.5  $K-2
163 5  1  1  $K-1  FORWARD CENTER CASE
164 1  0.5  $K-2
165 6  1  1  $K-1  AFT CENTER CASE
166 1  0.5  $K-2
167 7  1  1  $K-1  AFT ATTACH CASE ABOVE AND BELOW AFT ET RINGS
168 1  0.6  $K-2
169 8  1  1  $K-1  BETWEEN ET RINGS
170 1  0.62  $K-2
171 9  1  1  $K-1  AFT ET STUBS
172 1  0.4  $K-2
173 10  1  1  $K-1  AFT ATTACH CASE AND AFT SKIRT CYLINDER
174 1  0.56  $K-2
175 11  1  1  $K-1  AFT DOME
176 1  0.362 $K-2
177 12  1  1  $K-1  AFT SKIRT CONE
178 2  0.50  $K-2
179 13 1  3  $K-1  TANG/CLEVIS EQUIVALENT SHELL WALL
180 1  0.300 $K-2  INNER CLEVIS LUG
181 1  0.500 $K-2  TANG
182 1  0.300 $K-2  OUTER CLEVIS LUG
183 14  1  1  $K-1  AFT ET FLANGES
184 1  0.25  $K-2
185 C
186 C USER PARAMETERS
187 C
188 8  10  $L-1
189 C
```

```
190 C ET STUB SHELL UNIT NUMBERS,WALL TABLE FOR FLANGES,RING CAP
191 C TABLE, NUMBER OF COLUMNS, NUMBER OF FLANGE ELEMENTS, KQUAD
192 C NUMBER OF USER POINTS DEFINED ON CARDS
193 C
194 9  10  14  2  46  33  411 0  $L-2A  IUS1,IUS2,IWALL,ICROSS,NCOLS,NELT,KQUAD,NPTS
195 C
196 C GLOBAL AXIAL LOCATION OF ET STUBS, CIRCUMFERENTIAL ANGLE PER FLANGE ELEMENT
197 C
198 1304.02  1315.99  8.0,  $L-2B  XG1,XG2,DANGLE
199 988. 926. 910. 893. 887. 893. 907.  $L-2B P(1) TO P(7) SRM PRESSURE DIST.
200 C
201 C****************************************************
202 C
203 C SHELL UNIT DEFINITIONS
204 C
205 C****************************************************
206 C
207 C FORWARD CONE (UNIT 1)
208 C
209 6  0  $N-1 CONICAL SEGMENT
210 0.0  195.0  0.0  360.0  0.0  72.62  $N-2A
211 0  $N-5  SHELL WALL TYPE
212 411  $N-1 SELECT ELEMENT TYPE
213 6  6  6  6  $P-1
214 0  $Q-1 NO LOADS
215 1  1  0  0  0  1  $R-1
216 C
217 C FORWARD SKIRT CYLINDER (UNIT 2)
218 C FACTORY JOINT AT STATION 531
219 C FORWARD ET RING AT STATION 447.6
220 C
221 5  1  $N-1  CYLINDRICAL SEGMENT
222 0.0  135.48  0.0  360.0  72.62  $N-2A
223 0  $N-5  SHELL WALL TYPE
224 411  3  $N-1 SELECT ELEMENT TYPE
225 51.6  80.88  3.0  $N-2
226 3  6  1  $N-3
227 1  0.0  0.0  $O-1A FORWARD ET RING
228 4  1  46  $O-1B
229 CC 0  0  0  51.6  0.0  360.0  $O-1B
230 9  0.0  0.0  $O-1A  FWD ET LOAD INTRO RING
231 3  1  46  $O-1B
232 9  0.0  0.0  $O-1A  FWD ET LOAD INTRO RING
233 5  1  46  $O-1B
234 6  6  6  6  $P-1
235 C
236 C FORWARD ET STRUT LOADS
237 C
238 1  $Q-1
239 1  6  $Q-2
240 29885.1  1  3  4  23  1  $Q-3  PZ=-0.5*P15
241 29885.1  1  3  4  24  1  $Q-3  PZ
242 87428.05  1  2  4  23  1  $Q-3  PY=0.5*P16
243 87428.05  1  2  4  24  1  $Q-3  PY
244 212197.1  1  1  4  23  1  $Q-3  PX=-0.5*P14
245 212197.1  1  1  4  24  1  $Q-3  PX
246 1  1  0  0  0  1  $R-1
247 C
248 C FORWARD DOME (UNIT 3)
249 C
250 7  1  $N-1
251 0.0  63.35  0.0  360.0  81.25  $M-2A
252 0  $N-5  SHELL WALL TYPE
253 411  $N-1  SELECT ELEMENT TYPE
```

25

```
254 6  6  6  6  $P-1
255 1  $Q-1  LOAD CARDS
256 1  1  $Q-2
257 0.0  5  3  0  0  $Q-3  LIVE PRESSURE
258 1  1  0  0  0  1  $R-1
259 C
260 C FORWARD CASE STATION 531 TO 851 (UNIT 4)
261 C FACTORY/FIELD JOINTS AT STATIONS 531, 691 AND 851
262 C
263 5  1  $N-1
264 0.0  320.0  0.0  360.0  72.62  $M-2A CYLINDER
265 0  $N-5  SHELL WALL TYPE
266 411  5  $N-1  SELECT ELEMENT TYPE
267 3.0  154.0  6.0  154.0  3.0  $N-2
268 1      15      2      15      1  $N-3
269 6  6  6  6  $P-1
270 1  $Q-1
271 1  1  $Q-2
272 0.0  5  3  0  0  $Q-3  LIVE PRESSURE
273 1  1  0  0  0  1  $R-1
274 C
275 C FORWARD CENTER CASE FROM 851 TO 1171 (UNIT 5)
276 C FACTORY/FIELD JOINTS AT STATIONS 851, 1011 AND 1171
277 C
278 5  1  $N-1
279 0.0  320.0  0.0  360.0  72.62  $M-2A  CYLINDER
280 0  $N-5  SHELL WALL TYPE
281 411  5  $N-1 ELEMENT TYPE
282 3.0  154.0  6.0  154.0  3.0  $N-2
283 1      15      2      15      1  $N-3
284 6 6 6 6  $P-1
285 1  $Q-1
286 1  1  $Q-2
287 0.0  5  3  0  0  $Q-3  LIVE PRESSURE
288 1  1  0  0  0  1  $R-1
289 C
290 C AFT CENTER CASE FROM 1171 TO 1491 (UNIT 6)
291 C FACTORY/FIELD JOINTS AT STATIONS 1171, 1331 AND 1491
292 C
293 5  1  $N-1
294 0.0  320.0  0.0  360.0  72.62  $M-2A  CYLINDER
295 0  $M-5  SHELL WALL TYPE
296 411  5    $N-1 ELEMENT TYPE
297 3.0  154.0  6.0  154.0  3.0  $N-2
298 1  15      2  15      1  $N-3
299 6 6 6 6  $P-1
300 1  $Q-1
301 1  1  $Q-2
302 0.0  5  3  0  0  $Q-3  LIVE PRESSURE
303 1  1  0  0  0  1  $R-1
304 C
305 C AFT ATTACH CASE FROM 1491 TO 1505 (UNIT 7)
306 C SEGMENT ABOVE AFT ET RINGS
307 C
308 5  1  $N-1
309 0.0  13.54  0.0  360.0  72.62  $M-2A  CYLINDER
310 0  $M-5  SHELL WALL TYPE
311 411  2  $N-1 ELEMENT TYPE
312 3.0 10.54  $N-2
313 1      1  $N-3
314 6 6 6 6  $P-1
315 1  $Q-1
316 1  1  $Q-2
317 0.0  5  3  0  0  $Q-3  LIVE PRESSURE
```

```
318 1  1  0  0  0  1  $R-1
319 C
320 C SEGMENT BETWEEN ET ATTACHMENT FLANGES (UNIT 8)
321 C
322 5  1  $N-1  CYLINDRICAL PANEL
323 0.0  11.97  0.0  360.0  72.62  $N-2A
324 0  0  0.0  0.02  $N-5 SELECT WALL TYPE AND SET ECCENTRICITY
325 411  $N-1  SELECT ELEMENT TYPE
326 6  6  6  6  $P-1  BOUNDARY CONDITIONS
327 1  $Q-1  LOADS
328 1  1  $Q-2
329 0.0  5  3  0  0  $  LIVE PRESSURE LOADING
330 1  1  0  0  0  1  $R-1  PRINT OPTIONS
331 C
332 C UPPER ET ATTACHMENT FLANGE (UNIT 9)
333 C
334 4  1  $N-1  ANNULAR PLATE
335 72.62  74.2578  0.0  360.0  $N-2A
336 0  $N-5  SELECT WALL TYPE
337 411  $N-1  SELECT ELEMENT TYPE
338 6  6  3  6  $P-1  BOUNDARY CONDITIONS
339 0  $Q-1  LOADS
340 1  1  0  0  0  1  $R-1  PRINT OPTIONS
341 C
342 C LOWER ET ATTACHMENT FLANGE (UNIT 10)
343 C
344 4  1  $N-1  ANNULAR PLATE
345 72.62  74.2578  0.0 360.0  $N-2A
346 0  $N-5  SELECT WALL TYPE
347 411  $N-1  SELECT ELEMENT TYPE
348 6  6  3  6  $P-1  BOUNDARY CONDITIONS
349 0  $Q-1  NO LOADS
350 1  1  0  0  0  1  $R-1  PRINT OPTIONS
351 C
352 C SEGMENT BELOW AFT ET RING FROM 1517 TO 1577 (UNIT 11)
353 C FACTORY JOINT AT 1577
354 C
355 5  1  $N-1
356 0.0  60.49  0.0  360.0  72.62  $N-2A  CYLINDER
357 0  $N-5  SHELL WALL MODEL
358 411  2  $N-1  ELEMENT TYPE
359 57.49  3.0  $N-2
360 6      1    $N-3
361 6 6 6 6 $P-1
362 1  $Q-1
363 1  1  $Q-2
364 0.0  5  3  0  0  $Q-3  LIVE PRESSURE
365 1  1  0  0  0  1  $R-1
366 C
367 C AFT ATTACH CASE FROM 1577 TO 1824 (UNIT 12)
368 C FACTORY JOINTS AT 1577 AND 1697
369 C STUB RINGS AT 1613 AND 1657
370 C SPLASH DOWN RINGS AT 1733 AND 1777
371 C
372 5  1  $N-1
373 0.0  246.37  0.0  360.0  72.62  $N-2A  CYLINDER
374 0  $N-5  SHELL WALL TYPE
375 411  6  $N-1 ELEMENT TYPE
376 3.0  114.06  6.0  114.06  6.0  3.25  $N-2
377 1    12    2    12    2    1    $N-3
378 3  0.0  0.0  0.98  $O-1A  STUB RING AT 1613
379 0  0  0  36.15  0.0  360.0  $O-1B
380 3  0.0  0.0  0.98  $O-1A  STUB RING AT 1657
381 0  0  0  80.04  0.0  360.0  $O-1B
```

```
382 4 .0.0  0.0  2.6291 $O-1A  SPLASH DOWN RING AT 1733
383 0  0  0 156.21  0.0  360.0  $O-1B
384 4  0.0  0.0  2.6291 $O-1A  SPLASH DOWN RING AT 1777
385 0  0  0 200.23  0.0  360.0  $O-1B
386 6 6 6 6    $P-1
387 1  $Q-1
388 1  1  $Q-2
389 0.0  5  3  0  0  $Q-3  LIVE PRESSURE
390 1  1  0  0  0  1  $R-1
391 C
392 C AFT DOME (UNIT 13)
393 C
394 7  1  $N-1  SPHERICAL SHELL
395 90.0  133.49  0.0  360.0  72.62  $N-2A  SPHERICAL SHELL
396 0  $N-5  WALL TYPE
397 411  2  $N-1  ELEMENT TYPE
398 40.0  3.49  $N-2
399 8  1  $N-3
400 5  0.  0.  0.  $O-1A CASE BOSS
401 9  1  46  $O-1B
402 5  0.  0.  0.  $O-1A CASE BOSS
403 10  1  46  $O-1B
404 CC 0  0  0  133.49  0.  360.$O-1B
405 6 6 3 6  $P-1
406 0  $Q-1  NO LOADS
407 1  1  0  0  0  1  $R-1
408 C
409 C AFT SKIRT CYLINDER (UNIT 14)
410 C FACTORY JOINT AT STATION 1697
411 C
412 5  1  $N-1
413 0.0  13.24  0.0  360.0  72.62  $N-2A
414 0  $N-5  WALL TYPE
415 411  2  $N-1  SELECT ELEMENT TYPE
416 12.24  1.0  $N-2
417  1   1   $N-3
418 5  0.  0.  3.0  $O-1A KICK RING
419 2  1  46  $O-1B
420 5  0.  0.  3.0  $O-1A KICK RING
421 1  1  46  $O-1B
422 6  6  6  6  $P-1
423 0  $Q-1
424 1  1  0  0  0  1  $R-1
425 C
426 C AFT SKIRT CONE  (UNIT 15)
427 C
428 6  1  $N-1  CONICAL SHELL
429 0.0  93.09  0.0  360.0  72.62  104.10  $N-2A
430 0  $N-5  SELECT WALL TYPE
431 411 2  $N-1
432 3.09  90.0  $N-2
433  1    10  $N-3
434 5  0.  0.  3.0  $O-1A KICK RING
435 1  1  46  $O-1B
436 5  0.  0.  3.0  $O-1A KICK RING
437 2  1  46  $O-1B
438 CC 0  0  0  1.0  0.  360. $O-1B
439 C
440 6  0.  0.  -1.5  $CONE RINGS
441 4  1  46  $O-1B
442 6  0.  0.  -1.5  $CONE RINGS
443 5  1  46  $O-1B
444 CC 0  0  0  31.91  0.  360.  $O-1B
445 C
```

```
446 6  0.   0.   -1.5  $CONE RINGS
447 8  1   46   $0-1B
448 6  0.   0.   -1.5  $CONE RINGS
449 9  1   46   $0-1B
450 CC 0  0   0  62.11  0.   360.   $0-1B
451 C
452 6  0.   0.   -1.5  $CONE RINGS
453 11 1   46   $ 0-1B
454 6  0.   0.   -1.5  $CONE RINGS
455 12 1   46   $ 0-1B
456 CC 0  0   0  92.55  0.   360.   $0-1B
457 C
458 8  0.   0.   0.   $0-2A HOLD-DOWN POSTS
459 8  1   12   $0-2B
460 8  0.   0.   0.   $0-2A
461 7  1   12   $0-2B
462 CC 0  0   0  60.   0.   93.09  $0-2B
463 C
464 8  0.   0.   0.   $0-2A HOLD-DOWN POSTS
465 16 1   12   $0-2B
466 8  0.   0.   0.   $0-2A
467 15 1   12   $0-2B
468 CC 0  0   0  120.  0.   93.09  $0-2B
469 8  0.   0.   0.   $0-2A HOLD-DOWN POSTS
470 30 1   12   $0-2B
471 8  0.   0.   0.   $0-2A
472 31 1   12   $0-2B
473 CC 0  0   0  240.  0.   93.09  $0-2B
474 C
475 8  0.   0.   0.   $0-2A HOLD-DOWN POSTS
476 37 1   12   $0-2B
477 8  0.   0.   0.   $0-2A
478 38 1   12   $0-2B
479 CC 0  0   0  300.  0.   93.09  $0-2B
480 C
481 7  0.   0.   0.   $0-2A CONICAL SKIRT STRINGERS
482 0  0   0  0.   0.   93.09  $0-2B
483 C
484 7  0.   0.   0.   $0-2A CONICAL SKIRT STRINGERS
485 0  0   0  15. 0.   93.09  $0-2B
486 C
487 7  0.   0.   0.   $0-2A CONICAL SKIRT STRINGERS
488 0  0   0  30. 0.   93.09  $0-2B
489 C
490 7  0.   0.   0.   $0-2A CONICAL SKIRT STRINGERS
491 0  0   0  45. 0.   93.09  $0-2B
492 C
493 7  0.   0.   0.   $0-2A CONICAL SKIRT STRINGERS
494 0  0   0  60. 0.   93.09  $0-2B
495 C
496 7  0.   0.   0.   $0-2A CONICAL SKIRT STRINGERS
497 0  0   0  75. 0.   93.09  $0-2B
498 C
499 7  0.   0.   0.   $0-2A CONICAL SKIRT STRINGERS
500 0  0   0  90. 0.   93.09  $0-2B
501 C
502 7  0.   0.   0.   $0-2A CONICAL SKIRT STRINGERS
503 0  0   0  105. 0.   93.09  $0-2B
504 C
505 7  0.   0.   0.   $0-2A CONICAL SKIRT STRINGERS
506 0  0   0  120. 0.   93.09  $0-2B
507 C
508 7  0.   0.   0.   $0-2A CONICAL SKIRT STRINGERS
509 0  0   0  135. 0.   93.09  $0-2B
```

```
510 C
511 7  0.  0.  0.  $0-2A CONICAL SKIRT STRINGERS
512 0  0  0  150. 0.  93.09  $0-2B
513 C
514 7  0.  0.  0.  $0-2A CONICAL SKIRT STRINGERS
515 0  0  0  165. 0.  93.09  $0-2B
516 C
517 7  0.  0.  0.  $0-2A CONICAL SKIRT STRINGERS
518 0  0  0  180. 0.  93.09  $0-2B
519 C
520 7  0.  0.  0.  $0-2A CONICAL SKIRT STRINGERS
521 0  0  0  195. 0.  93.09  $0-2B
522 C
523 7  0.  0.  0.  $0-2A CONICAL SKIRT STRINGERS
524 0  0  0  210. 0.  93.09  $0-2B
525 C
526 7  0.  0.  0.  $0-2A CONICAL SKIRT STRINGERS
527 0  0  0  225. 0.  93.09  $0-2B
528 C
529 7  0.  0.  0.  $0-2A CONICAL SKIRT STRINGERS
530 0  0  0  240. 0.  93.09  $0-2B
531 C
532 7  0.  0.  0.  $0-2A CONICAL SKIRT STRINGERS
533 0  0  0  255. 0.  93.09  $0-2B
534 C
535 7  0.  0.  0.  $0-2A CONICAL SKIRT STRINGERS
536 0  0  0  270. 0.  93.09  $0-2B
537 C
538 7  0.  0.  0.  $0-2A CONICAL SKIRT STRINGERS
539 0  0  0  285. 0.  93.09  $0-2B
540 C
541 7  0.  0.  0.  $0-2A CONICAL SKIRT STRINGERS
542 0  0  0  300. 0.  93.09  $0-2B
543 C
544 7  0.  0.  0.  $0-2A CONICAL SKIRT STRINGERS
545 0  0  0  315. 0.  93.09  $0-2B
546 C
547 7  0.  0.  0.  $0-2A CONICAL SKIRT STRINGERS
548 0  0  0  330. 0.  93.09  $0-2B
549 C
550 7  0.  0.  0.  $0-2A CONICAL SKIRT STRINGERS
551 0  0  0  345. 0.  93.09  $0-2B
552 C
553 6 6 3 6  $P-1
554 1  $Q-1  LOADS
555 1  24  $Q-2
556 0.0  -1  1  12  7   $Q-3 PAD HOLD DOWN BOLTS
557 0.0  -1  1  12 16   $Q-3 PAD HOLD DOWN BOLTS
558 0.0  -1  1  12 31   $Q-3 PAD HOLD DOWN BOLTS
559 0.0  -1  1  12 37   $Q-3 PAD HOLD DOWN BOLTS
560 0.0  -1  2  12  7   $Q-3 PAD HOLD DOWN BOLTS
561 0.0  -1  2  12 16   $Q-3 PAD HOLD DOWN BOLTS
562 0.0  -1  2  12 31   $Q-3 PAD HOLD DOWN BOLTS
563 0.0  -1  2  12 37   $Q-3 PAD HOLD DOWN BOLTS
564 0.0  -1  3  12  7   $Q-3 PAD HOLD DOWN BOLTS
565 0.0  -1  3  12 16   $Q-3 PAD HOLD DOWN BOLTS
566 0.0  -1  3  12 31   $Q-3 PAD HOLD DOWN BOLTS
567 0.0  -1  3  12 37   $Q-3 PAD HOLD DOWN BOLTS
568 0.0  -1  1  12  8   $Q-3 PAD HOLD DOWN BOLTS
569 0.0  -1  1  12 15   $Q-3 PAD HOLD DOWN BOLTS
570 0.0  -1  1  12 30   $Q-3 PAD HOLD DOWN BOLTS
571 0.0  -1  1  12 38   $Q-3 PAD HOLD DOWN BOLTS
572 0.0  -1  2  12  8   $Q-3 PAD HOLD DOWN BOLTS
573 0.0  -1  2  12 15   $Q-3 PAD HOLD DOWN BOLTS
```

```
574 0.0   -1  2  12 30   $Q-3 PAD HOLD DOWN BOLTS
575 0.0   -1  2  12 38   $Q-3 PAD HOLD DOWN BOLTS
576 0.0   -1  3  12  8   $Q-3 PAD HOLD DOWN BOLTS
577 0.0   -1  3  12 15   $Q-3 PAD HOLD DOWN BOLTS
578 0.0   -1  3  12 30   $Q-3 PAD HOLD DOWN BOLTS
579 0.0   -1  3  12 38   $Q-3 PAD HOLD DOWN BOLTS
580 1   1   0   0   0  1   $R-1
581 C
582 C ELEMENT UNIT DATA
583 C
584 1   $U-1
585 1   8  $U-2
586 C TOP ET FLANGE
587 -20593.85   1  3   59  0  1   $Q-3   0.5 * P8
588 -46501.65   1  3   48  0  1   $Q-3   0.5 * P9
589 -1383.91    1  3   55  0  1   $Q-3   0.5 * P10 IN Zg DIRECTION
590 -4826.25    1  2   55  0  1   $Q-3   0.5 * P10 IN Yg DIRECTION
591 C BOTTOM ET FLANGE
592 -20593.85   1  3  127  0  1   $Q-3   0.5 * P8
593 -46501.65   1  3  116  0  1   $Q-3   0.5 * P9
594 -1383.91    1  3  123  0  1   $Q-3   0.5 * P10 IN Zg DIRECTION
595 -4826.25    1  2  123  0  1   $Q-3   0.5 * P10 IN Yg DIRECTION
596 1   1   0   $V-1
```

Appendix B: User-Written Subroutine WALL

```
1          SUBROUTINE WALL(IUNIT,KUNIT,XU,YU,ZU,ZETA,ECZ,ILIN,
2        +                      IPLAS)
3  C
4  C VARIABLE SHELL WALL PROPERTIES DOWN THE LENGTH OF THE
5  C ETA RING MODEL
6  C
7          COMMON/WALLX/JWALL
8  C
9  C JUMP TO IUNIT-TH SHELL UNIT
10 C
11         IF(IUNIT.EQ.1)  GO TO  101
12         IF(IUNIT.EQ.2)  GO TO  201
13         IF(IUNIT.EQ.3)  GO TO  301
14         IF(IUNIT.EQ.4)  GO TO  401
15         IF(IUNIT.EQ.5)  GO TO  501
16         IF(IUNIT.EQ.6)  GO TO  601
17         IF(IUNIT.EQ.7)  GO TO  701
18         IF(IUNIT.EQ.8)  GO TO  801
19         IF(IUNIT.EQ.9)  GO TO  901
20         IF(IUNIT.EQ.10) GO TO 1001
21         IF(IUNIT.EQ.11) GO TO 1101
22         IF(IUNIT.EQ.12) GO TO 1201
23         IF(IUNIT.EQ.13) GO TO 1301
24         IF(IUNIT.EQ.14) GO TO 1401
25         IF(IUNIT.EQ.15) GO TO 1501
26         JWALL=14
27 C
28 C FORWARD CONE (UNIT 1)
29 C
30   101   CONTINUE
31         JWALL=1
32         RETURN
33 C
34 C FORWARD SKIRT CYLINDER (UNIT 2)
35 C
36   201   CONTINUE
37         JWALL=2
38         IF(XU.GT.132.0) JWALL=13
39         RETURN
40 C
41 C FORWARD DOME (UNIT 3)
42 C
43   301   CONTINUE
44         JWALL=3
45         RETURN
46 C
47 C FORWARD CASE (UNIT 4)
48 C
49   401   CONTINUE
50         IF(XU.LE.3.0) JWALL=13
51         IF(XU.GT.3.0.AND.XU.LE.157.0) JWALL=4
52         IF(XU.GT.157.0.AND.XU.LE.163.0) JWALL=13
53         IF(XU.GT.163.0.AND.XU.LE.317.0) JWALL=4
54         IF(XU.GT.317.0) JWALL=13
55         RETURN
56 C
57 C FORWARD CENTER CASE (UNIT 5)
58 C
59   501   CONTINUE
60         IF(XU.LE.3.0) JWALL=13
61         IF(XU.GT.3.0.AND.XU.LE.157.0) JWALL=5
```

```
62         IF(XU.GT.157.0.AND.XU.LE.163.0) JWALL=13
63         IF(XU.GT.163.0.AND.XU.LE.317.0) JWALL=5
64         IF(XU.GT.317.0) JWALL=13
65         RETURN
66  C
67  C AFT CENTER CASE (UNIT 6)
68  C
69   601   CONTINUE
70         IF(XU.LE.3.0) JWALL=13
71         IF(XU.GT.3.0.AND.XU.LE.157.0) JWALL=6
72         IF(XU.GT.157.0.AND.XU.LE.163.0) JWALL=13
73         IF(XU.GT.163.0.AND.XU.LE.317.0) JWALL=6
74         IF(XU.GT.317.0) JWALL=13
75         RETURN
76  C
77  C AFT ATTACH CASE ABOVE ET STUBS (UNIT 7)
78  C
79   701   CONTINUE
80         JWALL=7
81         IF(XU.LE.3.0) JWALL=13
82         RETURN
83  C
84  C SEGMENT BETWEEN ET STUBS (UNIT 8)
85  C
86   801   CONTINUE
87         JWALL=8
88         RETURN
89  C
90  C UPPER ET STUB (UNIT 9)
91  C
92   901   CONTINUE
93         JWALL=9
94         RETURN
95  C
96  C LOWER ET STUB (UNIT 10)
97  C
98  1001   CONTINUE
99         JWALL=9
100         RETURN
101 C
102 C AFT ATTACH CASE BELOW ET STUBS (UNIT 11)
103 C
104 1101   CONTINUE
105         JWALL=7
106         IF(XU.GE.57.49) JWALL=13
107         RETURN
108 C
109 C AFT ATTACH CASE (UNIT 12)
110 C
111 1201   CONTINUE
112         IF(XU.LE.3.0) JWALL=13
113         IF(XU.GT.3.0.AND.XU.LE.117.06) JWALL=10
114         IF(XU.GT.117.06.AND.XU.LE.123.06) JWALL=13
115         IF(XU.GT.123.06.AND.XU.LE.237.12) JWALL=10
116         IF(XU.GT.237.12.AND.XU.LE.243.12) JWALL=13
117         IF(XU.GT.243.12) JWALL=10
118         RETURN
119 C
120 C AFT DOME (UNIT 13)
121 C
122 1301   CONTINUE
123         JWALL=11
124         RETURN
125 C
```

```
126 C AFT SKIRT CYLINDER (UNIT 14)
127 C
128 1401  CONTINUE
129       JWALL=10
130       IF(XU.GE.12.24) JWALL=13
131       RETURN
132 C
133 C AFT SKIRT CONE (UNIT 15)
134 C
135 1501  CONTINUE
136       JWALL=12
137 C
138 C EXIT
139 C
140       RETURN
141       END
```

Appendix C: User-Written Subroutine USRPT

```
  1          SUBROUTINE USRPT
  2 C
  3 C GENERATE USER POINTS FOR THE NON-SYMMETRIC AFT ET FLANGES
  4 C
  5          COMMON/UPI/ IUS1,IUS2,IWALL,ICROSS,NCOLS,NELT,KQUAD
  6          COMMON/UPF/ XG1,XG2,DANGLE
  7          COMMON/PIE/DTR,RTD,PI
  8 C
  9 C INITIALIZE SOME VARIABLES
 10 C
 11          IUVW=111
 12          IRUVW=111
 13          ISYS=0
 14          POW=0.0
 15          ANG1=32.0
 16          ANG2=296.0
 17          RADIUS=72.62+1.6378
 18          IF(NCOLS.EQ.181) RADIUS=72.6865+1.6378
 19 C        DANGLE=360.0/FLOAT(NCOLS-1)
 20 C
 21 C ET STUB EDGE OF UPPER AFT ET FLANGE
 22 C
 23          IUPT=0
 24          IUS=IUS1
 25          IRS=2
 26          DO 100 I=1,NCOLS
 27          ANGLE=(I-1)*DANGLE
 28          IF(ANGLE.LT.ANG1.OR.ANGLE.GT.ANG2) GO TO 100
 29          ICS=I
 30          IUPT=IUPT+1
 31          CALL NODE(IUPT,IUS,IRS,ICS,0.0,0.0,0.0,0,0,0,0.0)
 32  100     CONTINUE
 33 C
 34 C OUTSIDE EDGE OF UPPER AFT ET FLANGE
 35 C
 36          XG=XG1
 37          DO 200 I=1,NCOLS
 38          ANGLE=(I-1)*DANGLE
 39          IF(ANGLE.LT.ANG1.OR.ANGLE.GT.ANG2)      GO TO 200
 40          IF(ANGLE.GE.ANG1.AND.ANGLE.LT.51.0)     GO TO 110
 41          IF(ANGLE.GE.51.0.AND.ANGLE.LT.255.0)  GO TO 120
 42          IF(ANGLE.GE.255.0.AND.ANGLE.LT.262.0) GO TO 130
 43          IF(ANGLE.GE.262.0.AND.ANGLE.LT.270.0) GO TO 140
 44          IF(ANGLE.GE.270.0.AND.ANGLE.LT.276.5) GO TO 150
 45          IF(ANGLE.GE.276.5.AND.ANGLE.LT.283.0) GO TO 160
 46          IF(ANGLE.GE.283.0.AND.ANGLE.LT.287.5) GO TO 170
 47          IF(ANGLE.GE.287.5.AND.ANGLE.LE.ANG2)  GO TO 180
 48 C
 49  110    W=3.19+(7.22-3.19)/(51.0-ANG1)*(ANGLE-ANG1)
 50          GO TO 190
 51  120    W=7.22
 52          GO TO 190
 53  130    W=7.22+(6.79-7.22)/(262.-255.)*(ANGLE-255.)
 54          GO TO 190
 55  140    W=6.79+(5.96-6.79)/(270.-262.)*(ANGLE-262.)
 56          GO TO 190
 57  150    W=5.96+(4.98-5.96)/(276.5-270.)*(ANGLE-270.)
 58          GO TO 190
 59  160    W=4.98+(3.31-4.98)/(283.-276.5)*(ANGLE-276.5)
 60          GO TO 190
 61  170    W=3.31+(2.20-3.31)/(287.5-283.)*(ANGLE-283.)
```

35

```
62          GO TO 190
63   180    W=2.20+(1.25-2.20)/(ANG2-287.5)*(ANGLE-287.5)
64 C
65   190    CONTINUE
66          RBAR=RADIUS+W
67          ZG=RBAR*COS(DTR*ANGLE)
68          YG=RBAR*SIN(DTR*ANGLE)
69          IUPT=IUPT+1
70          CALL NODE(IUPT,0,0,0,XG,YG,ZG,IUVW,IRUVW,ISYS,POW)
71   200    CONTINUE
72 C
73 C ET STUB EDGE OF LOWER AFT ET FLANGE
74 C
75          IUS=IUS2
76          IRS=2
77          DO 1100 I=1,NCOLS
78          ANGLE=(I-1)*DANGLE
79          IF(ANGLE.LT.ANG1.OR.ANGLE.GT.ANG2) GO TO 1100
80          ICS=I
81          IUPT=IUPT+1
82          CALL NODE(IUPT,IUS,IRS,ICS,0.0,0.0,0.0,0,0,0,0.0)
83  1100    CONTINUE
84 C
85 C OUTSIDE EDGE OF LOWER AFT ET FLANGE
86 C
87          XG=XG2
88          DO 1200 I=1,NCOLS
89          ANGLE=(I-1)*DANGLE
90          IF(ANGLE.LT.ANG1.OR.ANGLE.GT.ANG2)      GO TO 1200
91          IF(ANGLE.GE.ANG1.AND.ANGLE.LT.51.0)     GO TO 1110
92          IF(ANGLE.GE.51.0.AND.ANGLE.LT.255.0)    GO TO 1120
93          IF(ANGLE.GE.255.0.AND.ANGLE.LT.262.0)   GO TO 1130
94          IF(ANGLE.GE.262.0.AND.ANGLE.LT.270.0)   GO TO 1140
95          IF(ANGLE.GE.270.0.AND.ANGLE.LT.276.5)   GO TO 1150
96          IF(ANGLE.GE.276.5.AND.ANGLE.LT.283.0)   GO TO 1160
97          IF(ANGLE.GE.283.0.AND.ANGLE.LT.287.5)   GO TO 1170
98          IF(ANGLE.GE.287.5.AND.ANGLE.LE.ANG2)    GO TO 1180
99 C
100  1110   W=3.19+(7.22-3.19)/(51.0-ANG1)*(ANGLE-ANG1)
101         GO TO 1190
102  1120   W=7.22
103         GO TO 1190
104  1130   W=7.22+(6.79-7.22)/(262.-255.)*(ANGLE-255.)
105         GO TO 1190
106  1140   W=6.79+(5.96-6.79)/(270.-262.)*(ANGLE-262.)
107         GO TO 1190
108  1150   W=5.96+(4.98-5.96)/(276.5-270.)*(ANGLE-270.)
109         GO TO 1190
110  1160   W=4.98+(3.31-4.98)/(283.-276.5)*(ANGLE-276.5)
111         GO TO 1190
112  1170   W=3.31+(2.20-3.31)/(287.5-283.)*(ANGLE-283.)
113         GO TO 1190
114  1180   W=2.20+(1.25-2.20)/(ANG2-287.5)*(ANGLE-287.5)
115 C
116  1190   CONTINUE
117         RBAR=RADIUS+W
118         ZG=RBAR*COS(DTR*ANGLE)
119         YG=RBAR*SIN(DTR*ANGLE)
120         IUPT=IUPT+1
121         CALL NODE(IUPT,0,0,0,XG,YG,ZG,IUVW,IRUVW,ISYS,POW)
122  1200   CONTINUE
123 C
124 C EXIT
125 C
```

```
126      RETURN
127      END
```

Appendix D: User-written Subroutine USRELT

```
1           SUBROUTINE USRELT
2  C
3  C GENERATE THE CONNECTIVITIES FOR THE AFT ET FLANGES
4  C
5           COMMON/UPI/IUS1,IUS2,IWALL,ICROSS,NCOLS,NELT,KQUAD
6  C
7  C INITIALIZE SOME VARIABLES
8  C
9           ZETA=0.0
10          ECZ=0.0
11          ILIN=0
12          IPLAS=0
13          INTEG=0
14          IPENL=0
15          ANG1=32.0
16          ANG2=296.0
17 C        DANGLE=360.0/FLOAT(NCOLS-1)
18 C        NELT=INT((ANG2-ANG1)/DANGLE)
19          IF(KQUAD.EQ.410) KBM=210
20          IF(KQUAD.EQ.411) KBM=211
21          XSI=0.0
22          ECYB=0.0
23          ECZB=0.0
24 C
25 C MESH FOR UPPER ET FLANGE
26 C
27          DO 100 I=1,NELT
28          N1=I
29          N2=I+1
30          N3=NELT+1+I+1
31          N4=NELT+1+I
32          CALL QUAD(N1,N2,N3,N4,KQUAD,IWALL,ZETA,ECZ,
33        1 ILIN,IPLAS,INTEG,IPENL)
34 C
35 C ADD BOLT-ON RING CAPS
36 C
37          NR=N1
38          CALL BEAM(N4,N3,NR,KBM,ICROSS,XSI,ECYB,ECZB,ILIN,
39        1 IPLAS)
40 100      CONTINUE
41 C
42 C MESH FOR LOWER ET FLANGE
43 C
44          NNUF=2*(NELT+1)
45          DO 1100 I=1,NELT
46          N1=I+NNUF
47          N2=I+1+NNUF
48          N3=NELT+1+I+1+NNUF
49          N4=NELT+1+I+NNUF
50          CALL QUAD(N1,N2,N3,N4,KQUAD,IWALL,ZETA,ECZ,
51        1 ILIN,IPLAS,INTEG,IPENL)
52 C
53 C ADD BOLT-ON RING CAPS
54 C
55          NR=N1
56          CALL BEAM(N4,N3,NR,KBM,ICROSS,XSI,ECYB,ECZB,ILIN,
57        1 IPLAS)
58 C
59 1100     CONTINUE
60 C
61 C EXIT
```

```
62 C
63        RETURN
64        END
```

Appendix E: User-Written Subroutine UPRESS

```
1           SUBROUTINE UPRESS(T,PA,PB,IUNIT,IELT,X,Y,Z,LIVE,PRESS)
2  C
3  C VARIABLE SRM PRESSURE DISTRIBUTION
4  C
5           COMMON/UPI/ IUS1,IUS2,IWALL,ICROSS,NCOLS,NELT,KQUAD,NPTS
6           COMMON/UPF/ XG1,XG2,DANGLE,P(7)
7  C
8           LIVE=1
9           SEGLEN=320.0
10 C
11          IF(IUNIT.LT.3)RETURN
12          IF(IUNIT.EQ.9.OR.IUNIT.EQ.10) RETURN
13          IF(IUNIT.GE.13) RETURN
14 C
15 C PRESSURIZED SRM UNITS
16 C
17          IF(IUNIT.EQ.3)  GO TO 30
18          IF(IUNIT.EQ.4)  GO TO 40
19          IF(IUNIT.EQ.5)  GO TO 50
20          IF(IUNIT.EQ.6)  GO TO 60
21          IF(IUNIT.EQ.7)  GO TO 70
22          IF(IUNIT.EQ.8)  GO TO 80
23          IF(IUNIT.EQ.11) GO TO 110
24          IF(IUNIT.EQ.12) GO TO 120
25 C
26 C FORWARD DOME - UNIT 3
27 C
28 30       CONTINUE
29          PRESS=P(1)*PA
30          RETURN
31 C
32 C FORWARD CASE - UNIT 4
33 C
34 40       CONTINUE
35          SLOPE=(P(2)-P(1))/SEGLEN
36          PRESS=PA*(P(1)+SLOPE*X)
37          RETURN
38 C
39 C FORWARD CENTER CASE - UNIT 5
40 C
41 50       CONTINUE
42          SLOPE=(P(3)-P(2))/SEGLEN
43          PRESS=PA*(P(2)+SLOPE*X)
44          RETURN
45 C
46 C AFT CENTER CASE - UNIT 6
47_C
48 60       CONTINUE
49          SLOPE=(P(4)-P(3))/SEGLEN
50          PRESS=PA*(P(3)+SLOPE*X)
51          RETURN
52 C
53 C SEGMENT ABOVE AFT ET RINGS - UNIT 7
54 C
55 70       CONTINUE
56          SLOPE=(P(5)-P(4))/13.54
57          PRESS=PA*(P(4)+SLOPE*X)
58          RETURN
59 C
60 C SEGMENT BETWEEN AFT ET RINGS - UNIT 8
61 C
```

```
62 80      CONTINUE
63         PRESS=PA*P(5)
64         RETURN
65 C
66 C SEGMENT BELOW AFT ET RINGS - UNIT 11
67 C
68 110     CONTINUE
69         PRESS=PA*P(5)
70         RETURN
71 C
72 C AFT ATTACH CASE - UNIT 12
73 C
74 120     CONTINUE
75         IF(X.GT.206.37) GO TO 121
76         SLOPE=(P(6)-P(5))/206.37
77         PRESS=PA*(P(5)+SLOPE*X)
78         RETURN
79   121   SLOPE=(P(7)-P(6))/40.0
80         PRESS=PA*(P(6)+SLOPE*PA)
81         RETURN
82 C
83 C EXIT
84 C
85         END
```

References

1. SRB Integration Branch, Space Shuttle Systems Division: *SRB Systems Data Book, Volume 1*. SE-019-083-2H, NASA George C. Marshall Space Flight Center, June 1977 (Revision A).

2. *Report of the Presidential Commission on the Space Shuttle Challenger Accident*, Washington, D.C., June 6, 1986.

3. Greene, William H.; Knight, Norman F., Jr.; and Stockwell, Alan E.: *Structural Behavior of the Space Shuttle SRM Tang-Clevis Joint*, NASA TM-89018, September 1986.

4. Almroth, B. O.; Brogan, F. A.; and Stanley, G. M.: *Structural Analysis of General Shells, Vol. II, User Instructions for STAGSC-1*, Report No. LMSC-D633873, Lockheed Palo Alto Research Laboratory, Palo Alto, CA, December 1982.

5. Rankin, C. C.; Stehlin, P.; and Brogan, F. A.: *Enhancements to the STAGS Computer Code*, NASA CR-4000, November 1986.

6. Oostyen, J. E.; Bright, D. D.; Hawkins, G. F.; McCluskey, P. M.; and Larsen, G. L.: *SRM Joint Deflection Referee Test: Phase 2 Final Report*, Morton Thiokol, Inc., Wasatch Operations, Document Number TWR-300149, April 3, 1986.

7. Knight, Norman F., Jr.: *Nonlinear Shell Analyses of the SRB/ETA Ring Interface*, NASA TM-89164, July 1987.

8. Stein, S. R.: *Space Shuttle High Performance Motor SRM Case Stress Analysis*, Morton Thiokol, Inc., Wasatch Operations, Document Number TWR-12968 Rev. A, January 10, 1983.

9. Bailey, F. R.: NAS — Current Status and Future Plans. *Supercomputing in Aerospace*, NASA CP-2454, pp. 13-21, 1987.

10. Green, James L.; Thomas, Valerie L.; Lopez-Swafford, Brian; and Porter, Linda Z.: *Introduction to the Space Physics Analysis Network (SPAN)*, National Space Science Data Center Technical Report 87-04, January 1987.

11. Weiler, F. C.: Porting CFT/COS to CFT77/UNICOS/C. In Proceedings of the Fall 1986 Users Group Meeting held at Garmisch-Partenkirchen, West Germany, September 29 - October 3, 1986.

12. Dynamic Response and Loads Branch, Structural Dynamics Division: *Space Shuttle Solid Rocket Booster Design Loads: Book 1 — Prelaunch Through Separation*, SE-019-057-2H, NASA George C. Marshall Space Flight Center, May 1985 (Revision B).

Table 1. Time-Consistent SRB/ET Interface Loads.

ET STRUT LOADS, lbs.	Time after SSME Ignition, secs.			
	0.0	5.3	6.6	7.2
P8	98,394	41,188	53,639	109,626
P9	80,397	93,003	88,198	65,442
P10	47,834	-10,042	14,525	-22,958
P14	-971,398	-424,394	-422,609	-946,084
P15	-104,089	-59,770	-59,065	-33,267
P16	-42,618	174,856	80,639	38,454

Table 2. STAGSC-1 Performance Comparison on NAS Computers.

	Cray X-MP/12 COS, CPU Seconds	Cray-2 UNICOS CPU Seconds	
		No Vector Library	Vector Library
STAGS1	107	137	142
STAGS2	781	1577	853
TOTAL	888	1714	995

Table 3. CPU Performance of Various Classes of Computer Systems Using the STAGSC-1 Computer Program.

	VAX 11/785 VMS 4.5, CPU Seconds	CDC 173 NOS 2.4, CPU Seconds	CDC 855 NOS 2.4, CPU Seconds	CRAY-2 UNICOS 2.0, CPU Seconds
Form and Assemble Global Stiffness Matrix	901	478	96	18
Decompose the Global Stiffness Matrix	18536	9917	1983	96
Forward/Backward Substitution and Stress Recovery	514	236	47	7
Total	19951	10631	2126	121
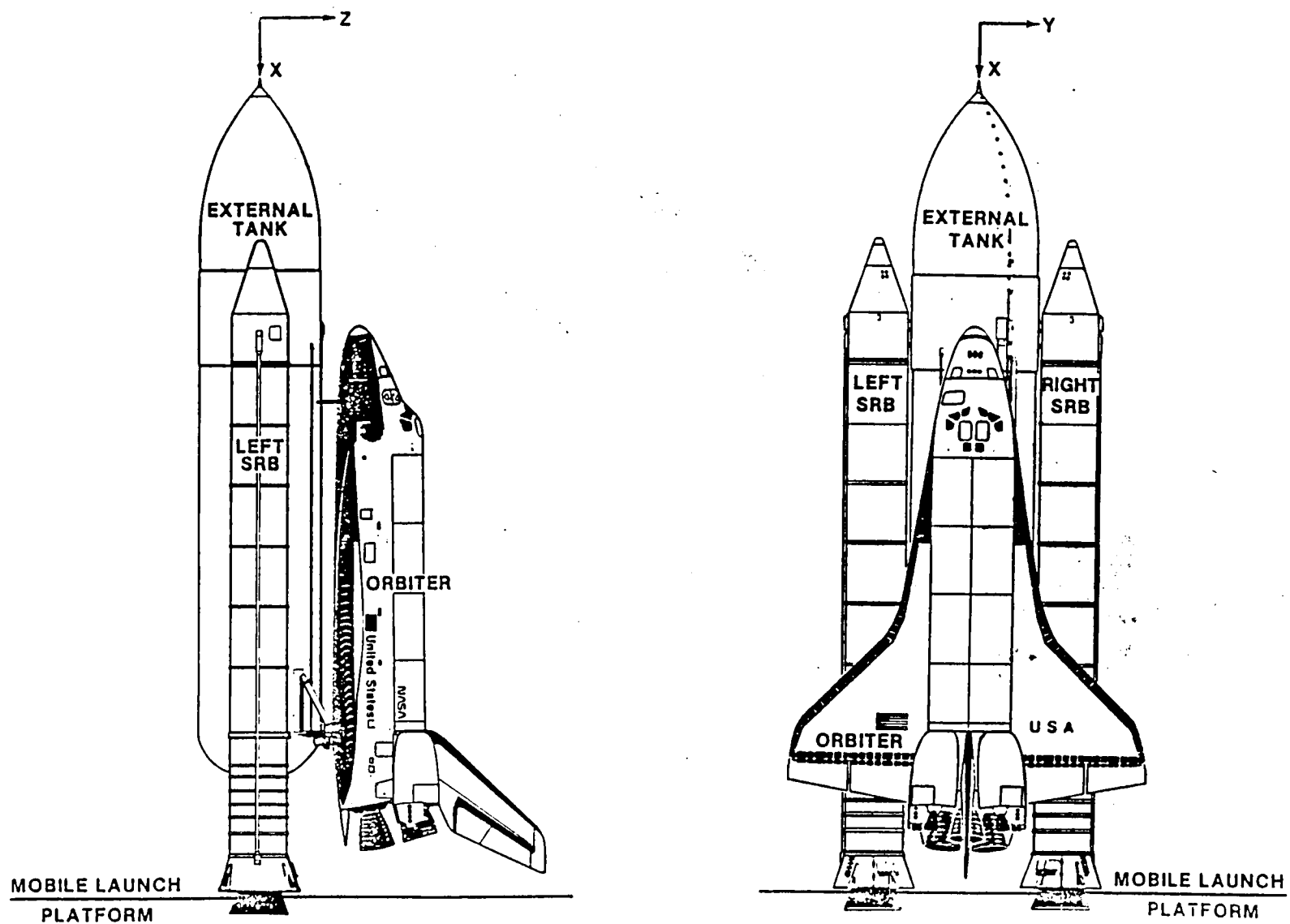
Fig. 1 Space Shuttle system.
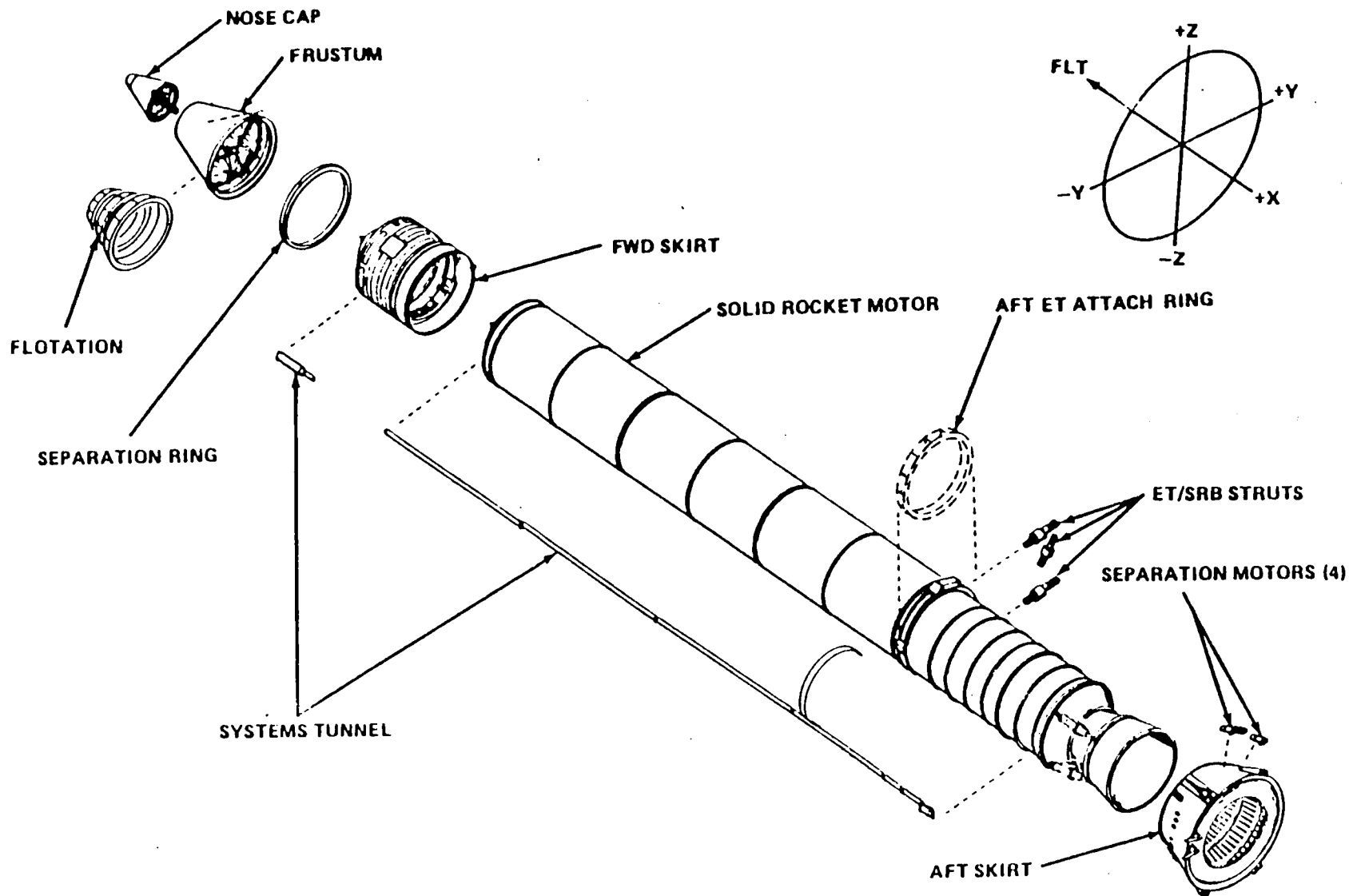
Fig. 2 SRB structural subsystems (figure 2-1 from reference 1).
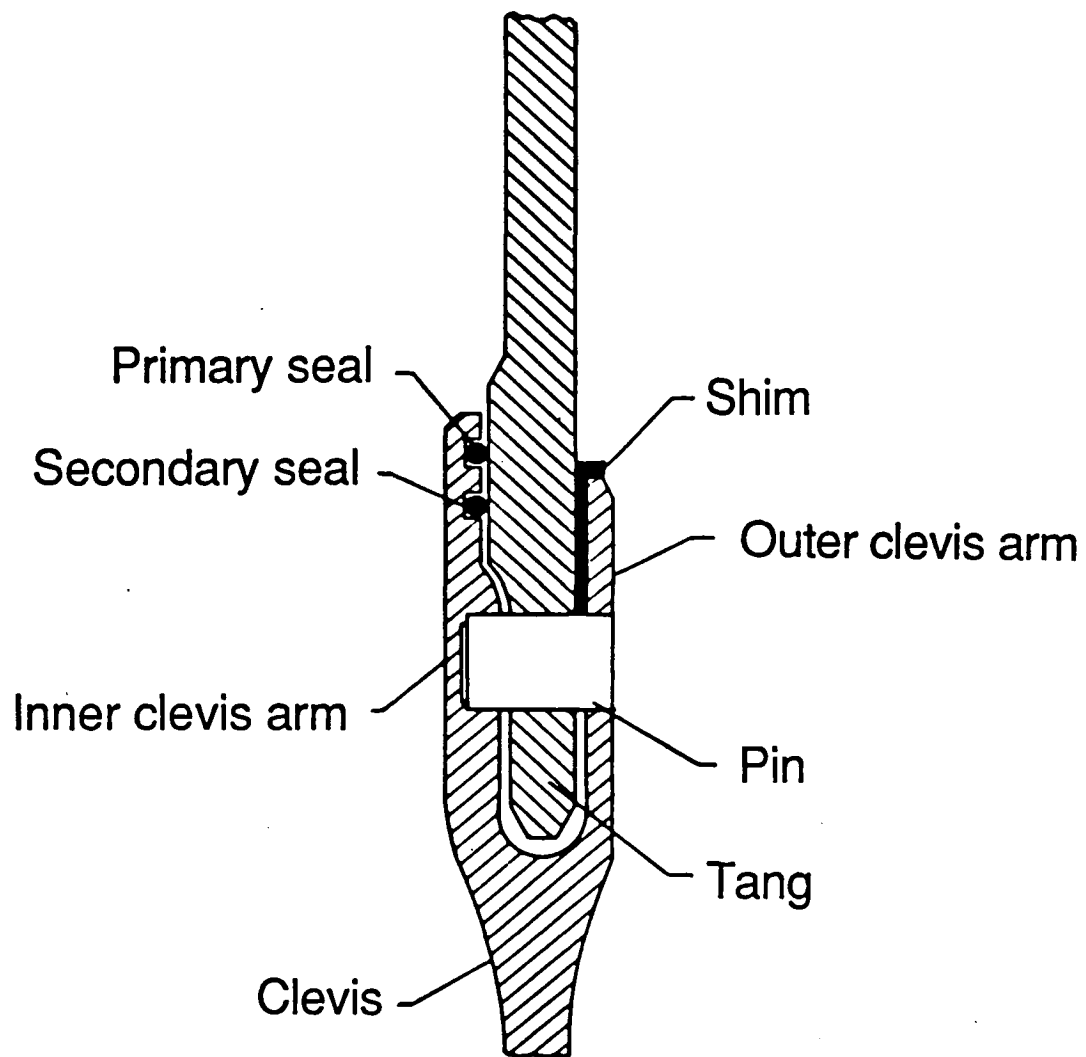
Fig. 3 Solid rocket motor case joint cross section.

Primary seal

Secondary seal

Inner clevis arm

Clevis

Shim

Outer clevis arm

Pin

Tang

2-D shell model of SRB with equivalent joints

3-D solid model of joint

2-D shell model of joint
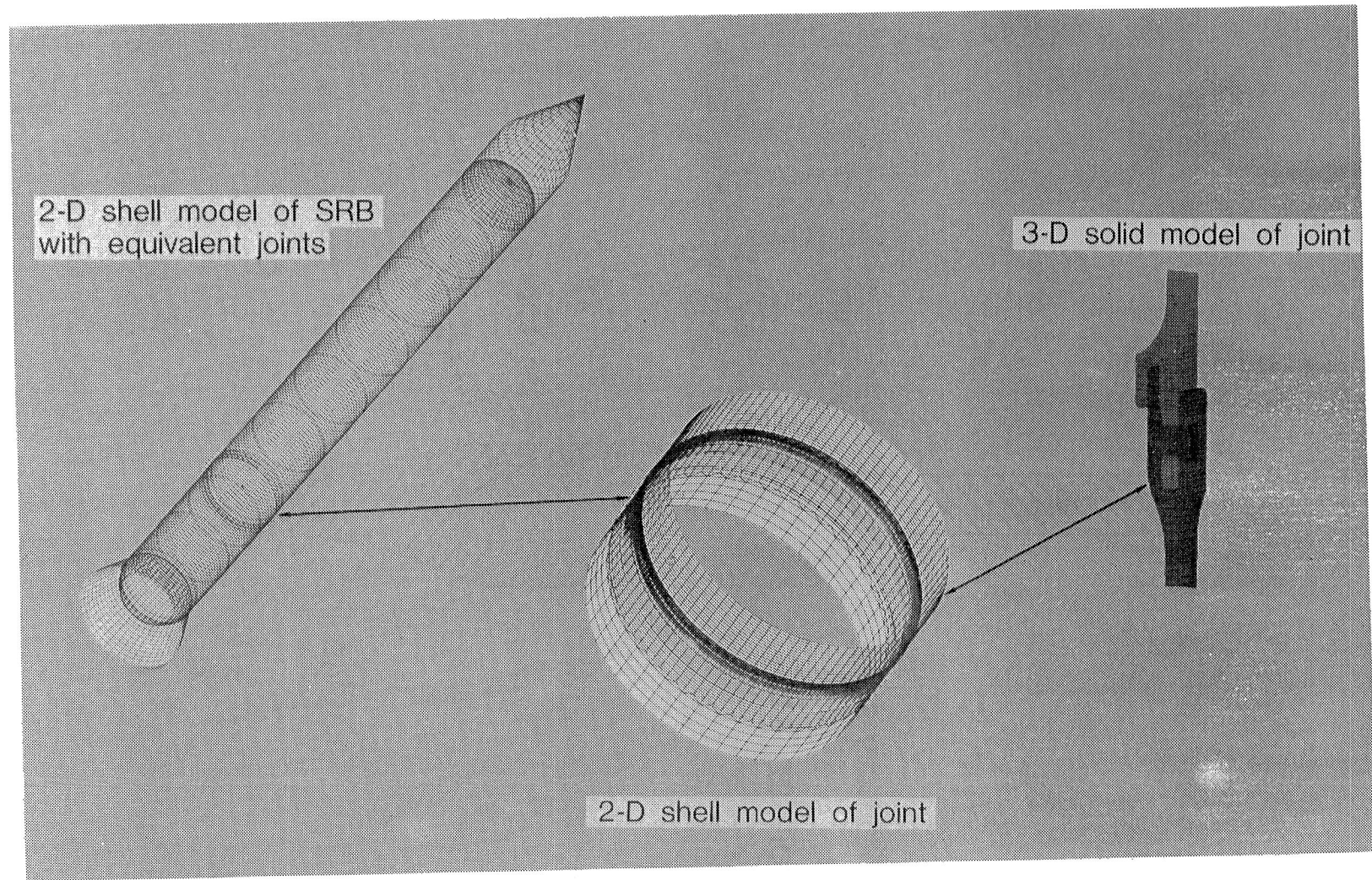
Fig. 4 Levels of SRB analysis.
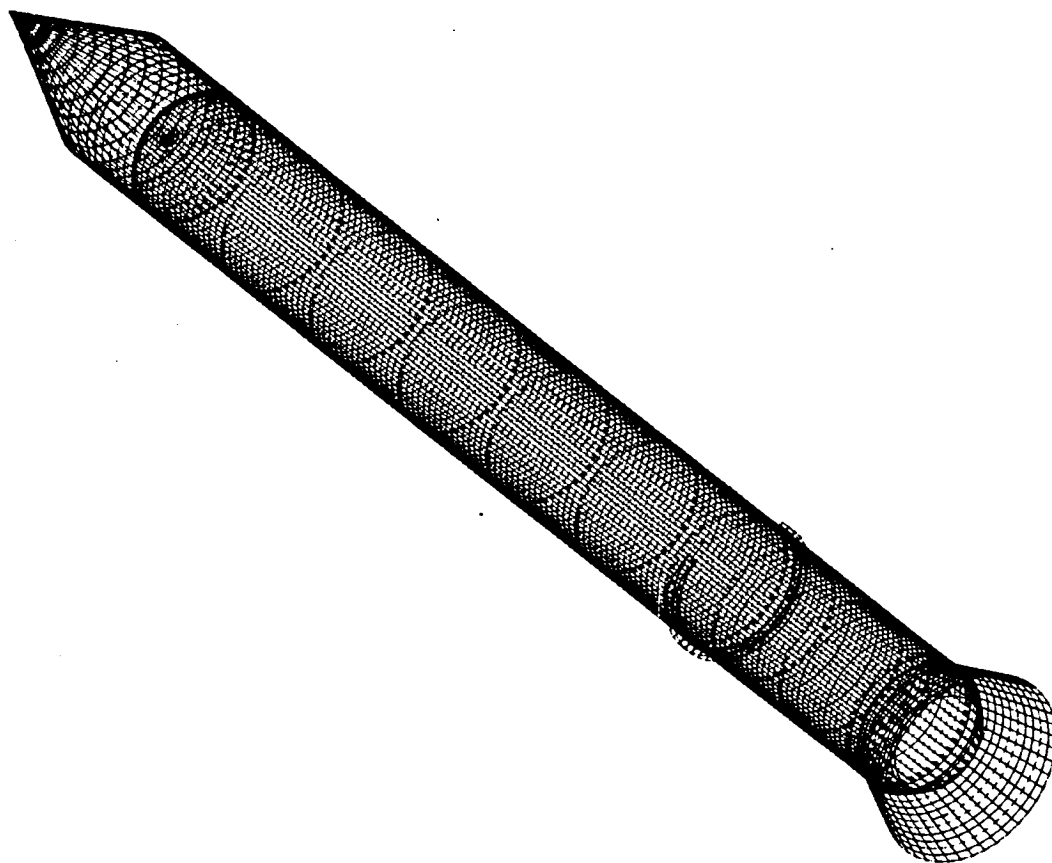
Fig. 5 Overall finite element model of SRB.

MAIN PARACHUTES

DROGUE PARACHUTE

IGNITER
STA 485

SEPARATION MOTORS

FORWARD SRB-ET
ATTACHMENT POINTS
STA 531

PROPELLANT BORE

FACTORY JOINT
STA 691

FIELD JOINT
STA 851

FACTORY JOINT
STA 1011

FIELD JOINT
STA 1171

FACTORY JOINT
STA 1331

FIELD JOINT
STA 1491

AFT SRB-ET
ATTACHMENT
POINTS

STA 1511

RING STIFFENER
STA 1613

FACTORY JOINT
STA 1577

RING STIFFENER
STA 1733

FACTORY JOINT
STA 1697

RING STIFFENER
STA 1777

FACTORY JOINT
STA 1812

NOZZLE

AFT SKIRT
STA 1837

SEPARATION MOTORS

Fig. 6 Details of SRB subsystem.
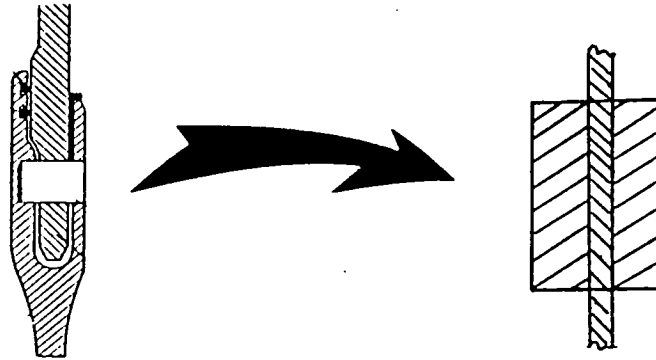
Fig. 7 Equivalent joint geometry.
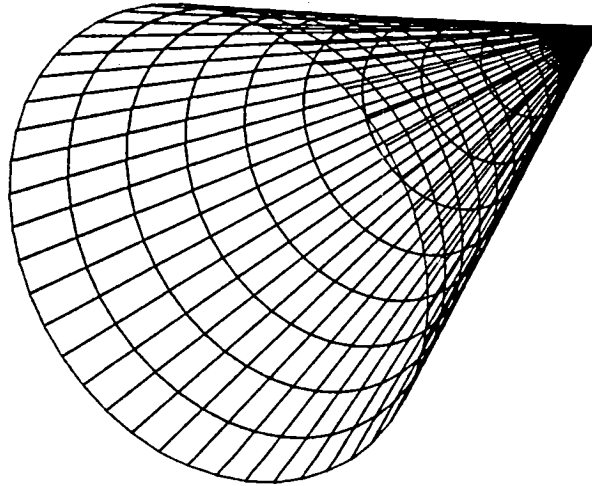
Fig. 8 Finite element model of forward cone.
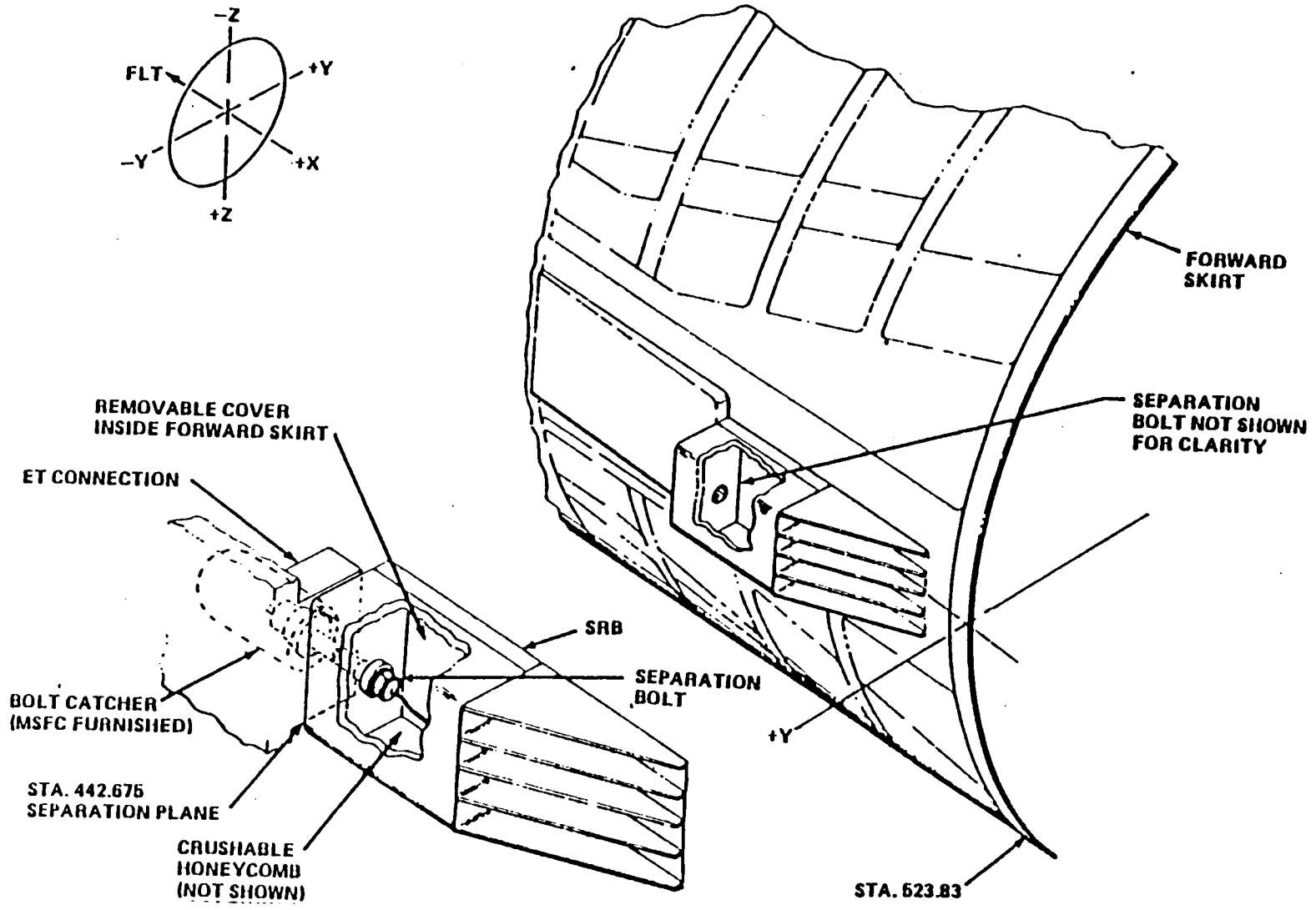
Fig. 9 SRB forward ET attachment (figure 2-7 from reference 1).
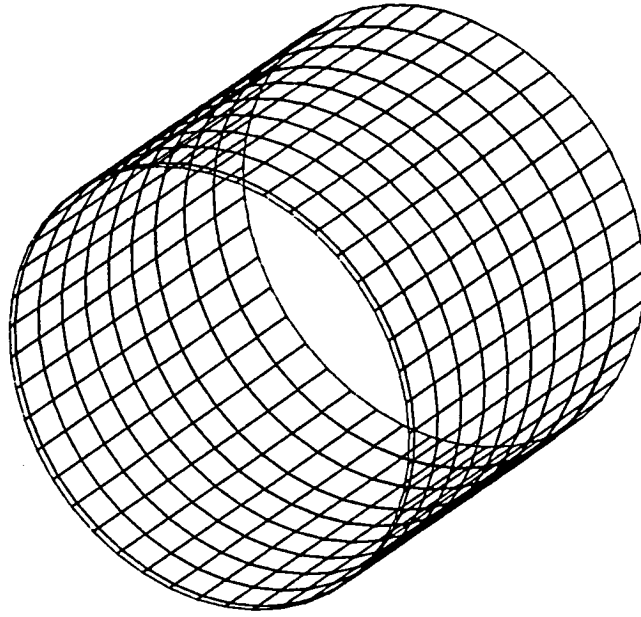
Fig. 10 Finite element model of forward skirt.
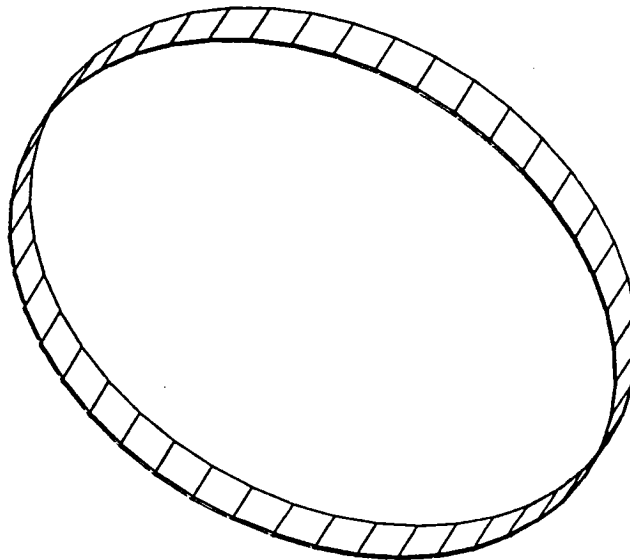
Fig. 11 Finite element model of aft cylinder skirt.
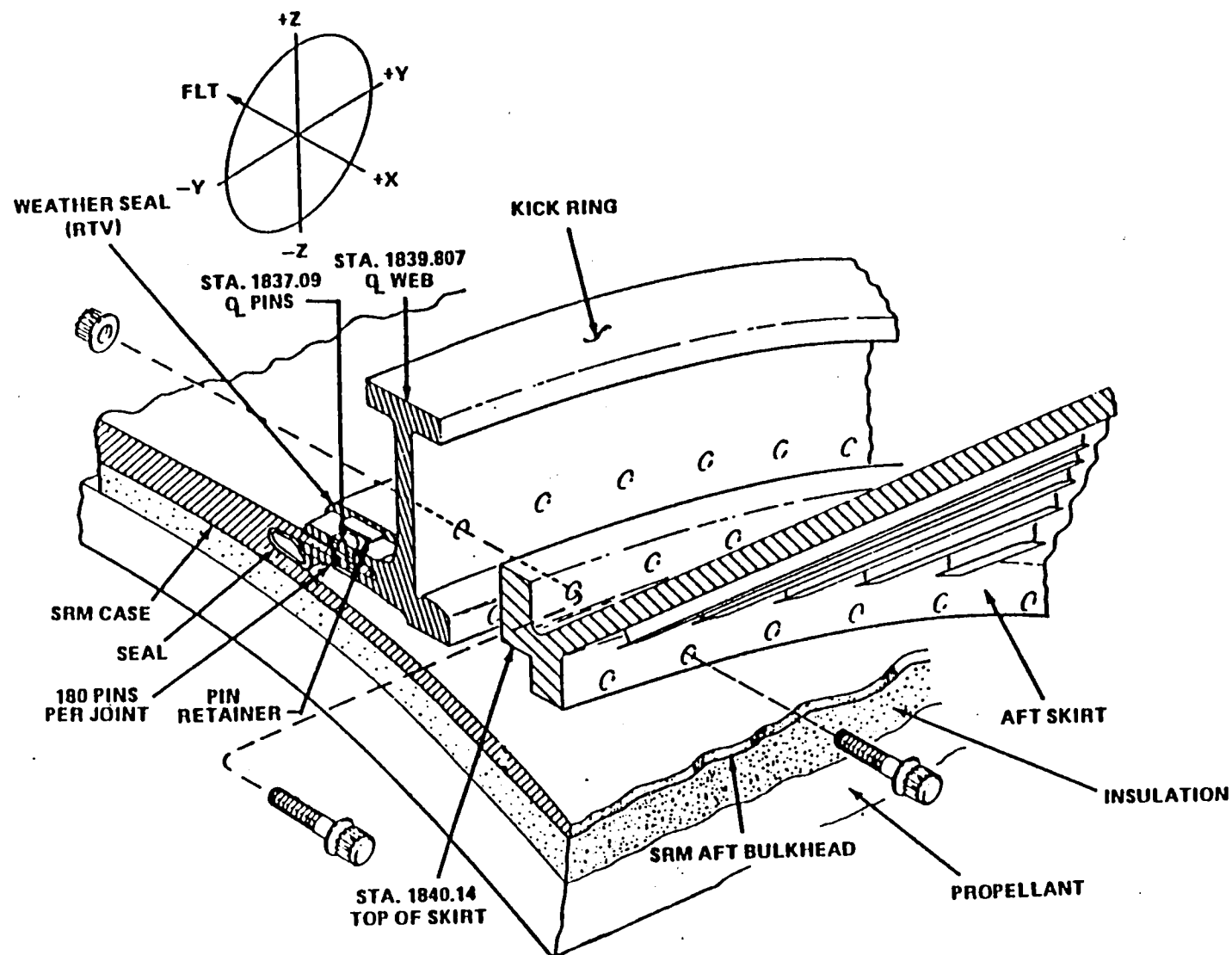
Fig. 12 Kick ring (figure 2-16 from reference 1).

Fig. 13 Aft skirt.

SEPARATION PLANE

BOOSTER CARTRIDGE TYP. 2 PLACES

FRANGIBLE NUT

WASHER

AFT SKIRT POST

AFT BSM (4)

HOLDDOWN POST (4)

AFT SKIRT

NON–METALLIC SHIM (EPON 934)

STEEL FOOT PAD

KSC SUPPORT POST

FOOT PAD RETAINER

BALL

STUD

NON–FLIGHT ITEMS

NOTE:
DEBRIS AND FOOT PAD RETAINERS OMITTED FOR CLARITY.

FLIGHT

BLAST CONTAINER

NSI DETONATOR AND BOOSTER

SPHERICAL WASHER

SRB SUPPORT POST

CASTABLE EPON 934

SEPARATION PLANE

SUPPORT POST BALL FITTING

SRB SKIRT SHOE

CABLE

MLP SUPPORT POST

FRANGIBLE NUT & BOOSTER CARTRIDGE

NON–METALLIC SHIM (EPON 934)

HOLD DOWN STUD

NUT & WASHERS

STACKING CONFIG. TYP 4 PLACES

Fig. 14 SRB aft skirt holddown connection at MLP (figure 2-15 from reference 1).

58
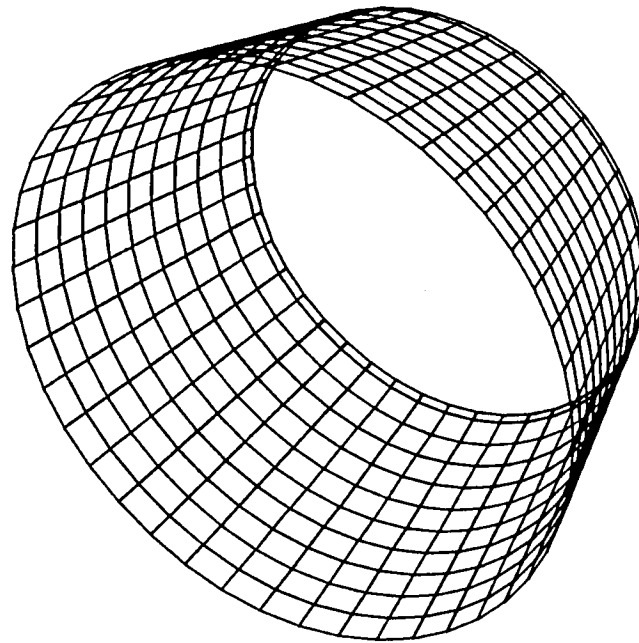
Fig. 15 Finite element model of aft conical skirt.

ET ATTACH RING

SHORT
RING
SEGMENT

IEA COVER

LONG
RING
SEGMENT

IEA END COVER
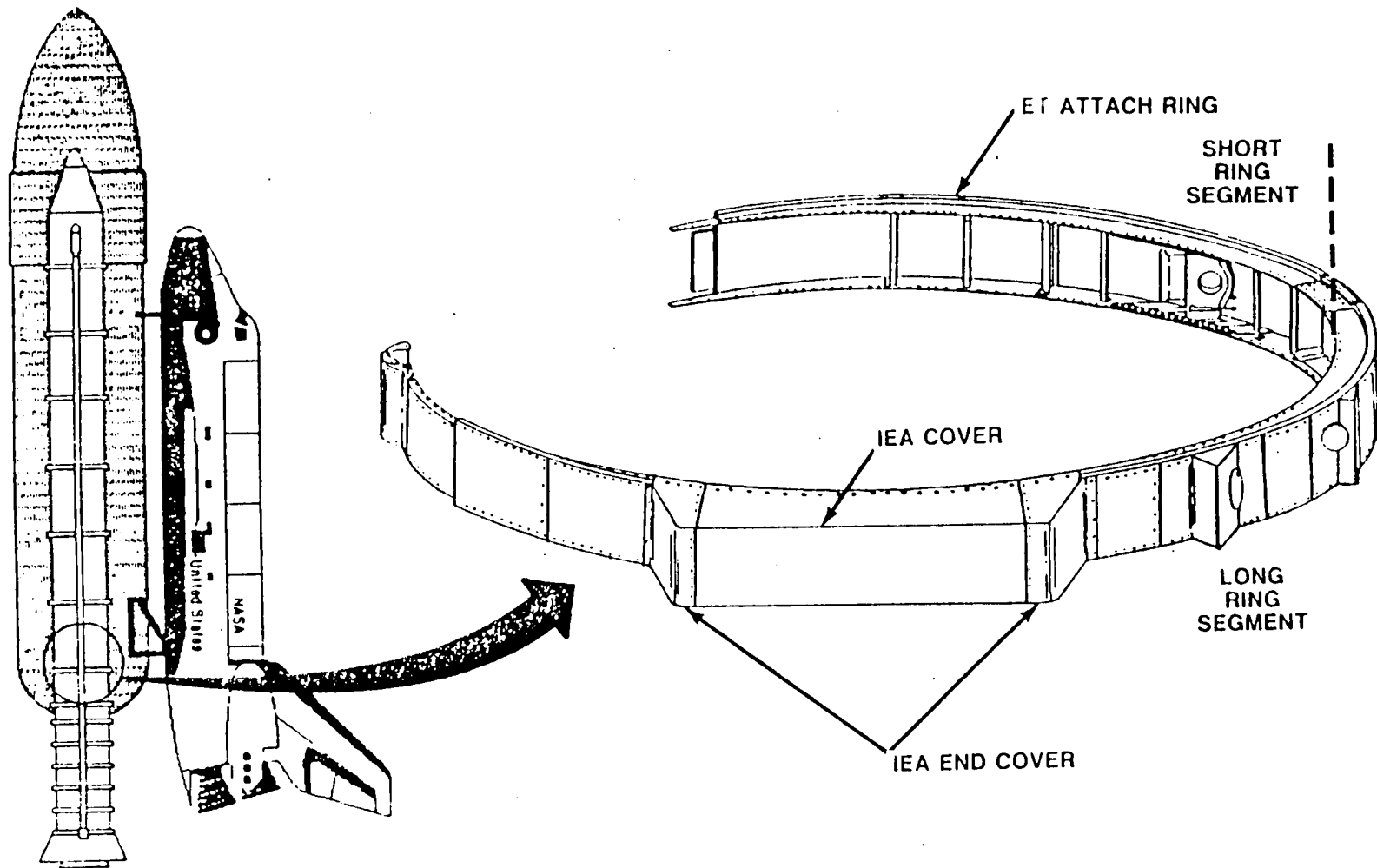
Fig. 16 Aft ETA ring assembly.
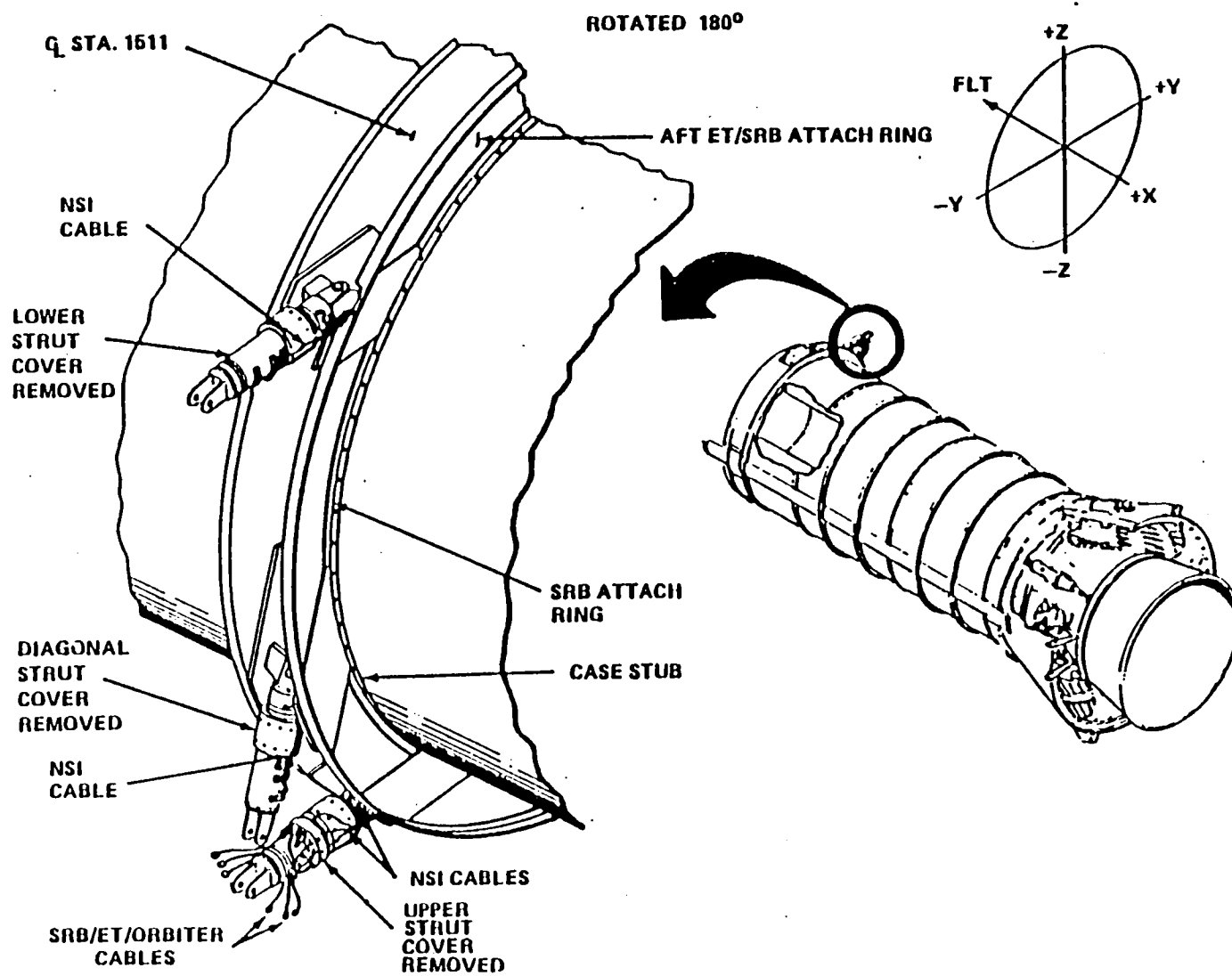
Fig. 17 Aft ET struts (figure 2-8 from reference 1).
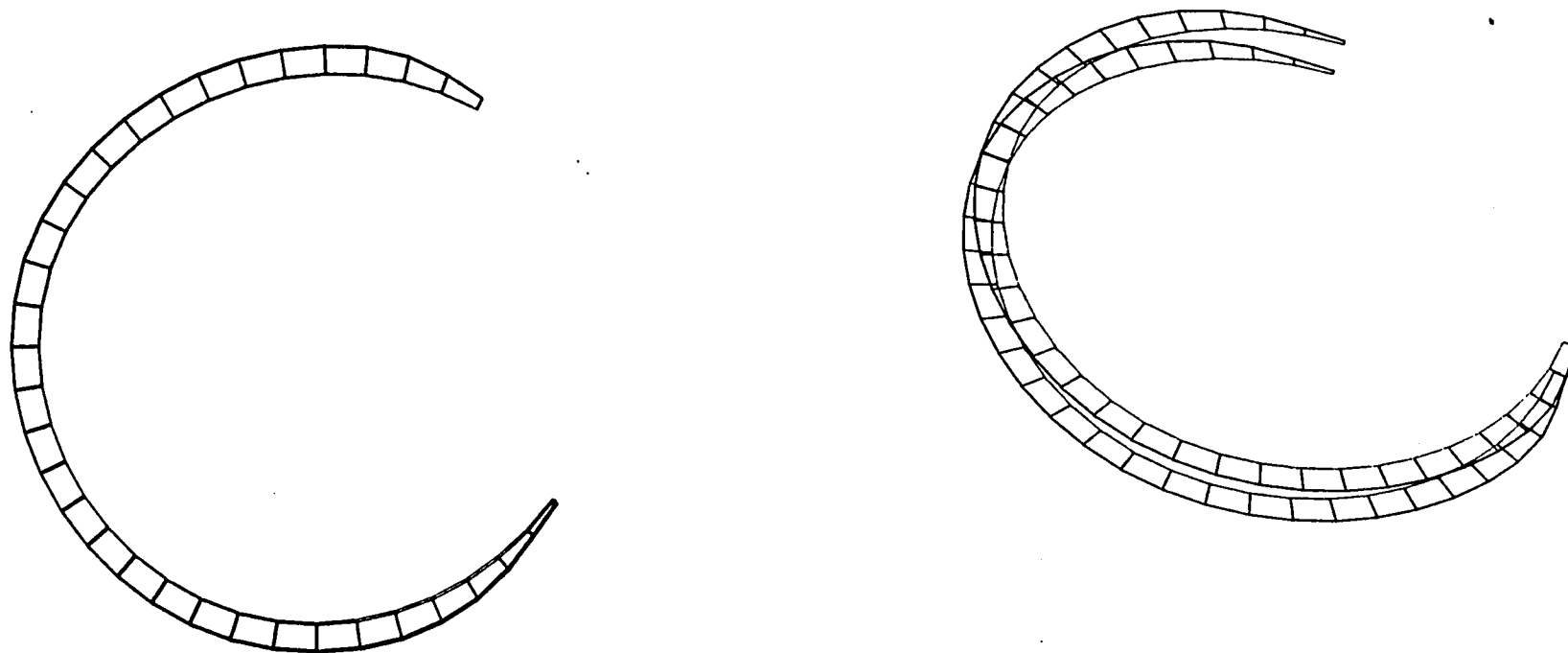
Fig. 18 Finite element model of ETA ring.
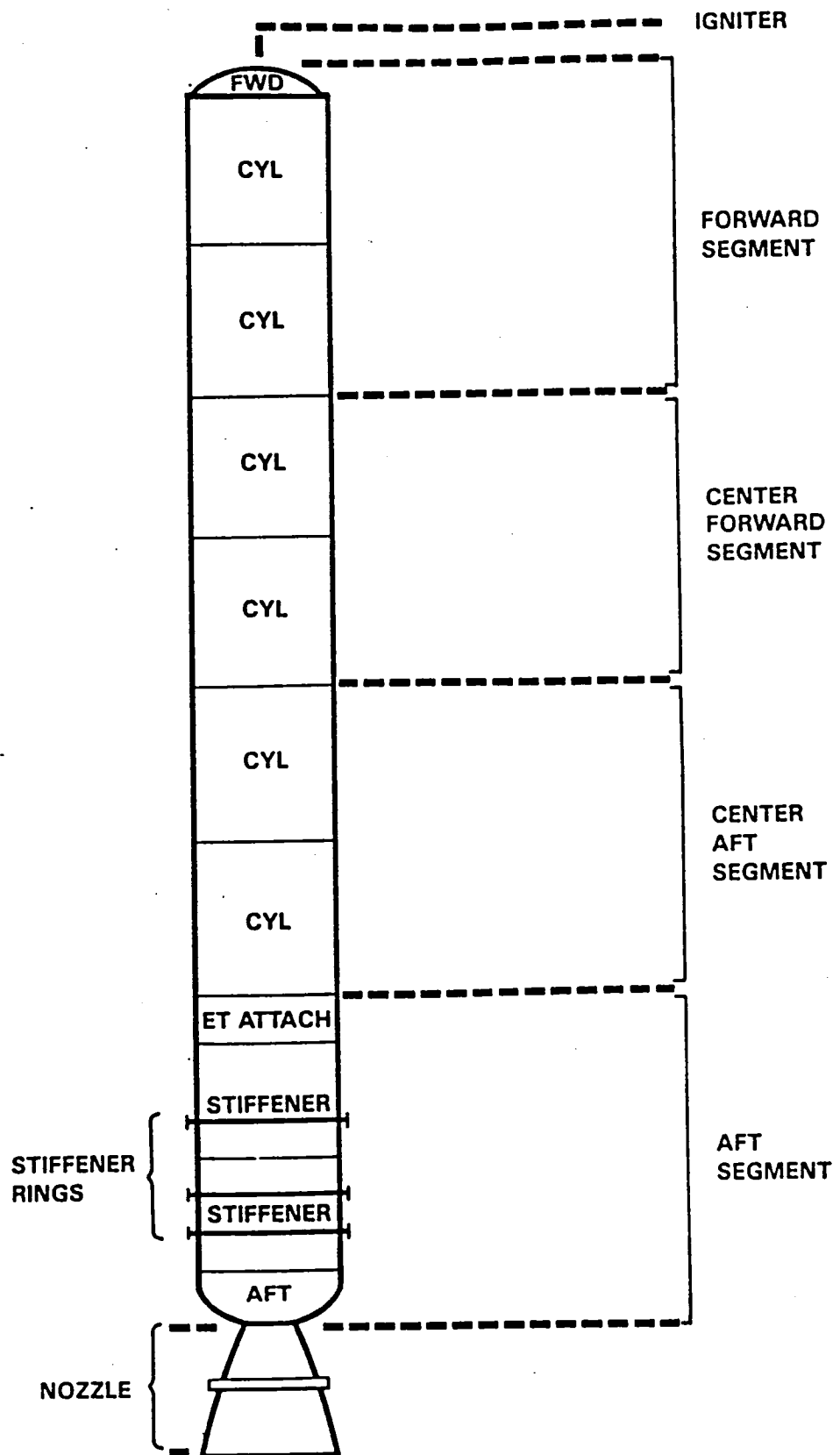
Fig. 19 SRM motor segments.
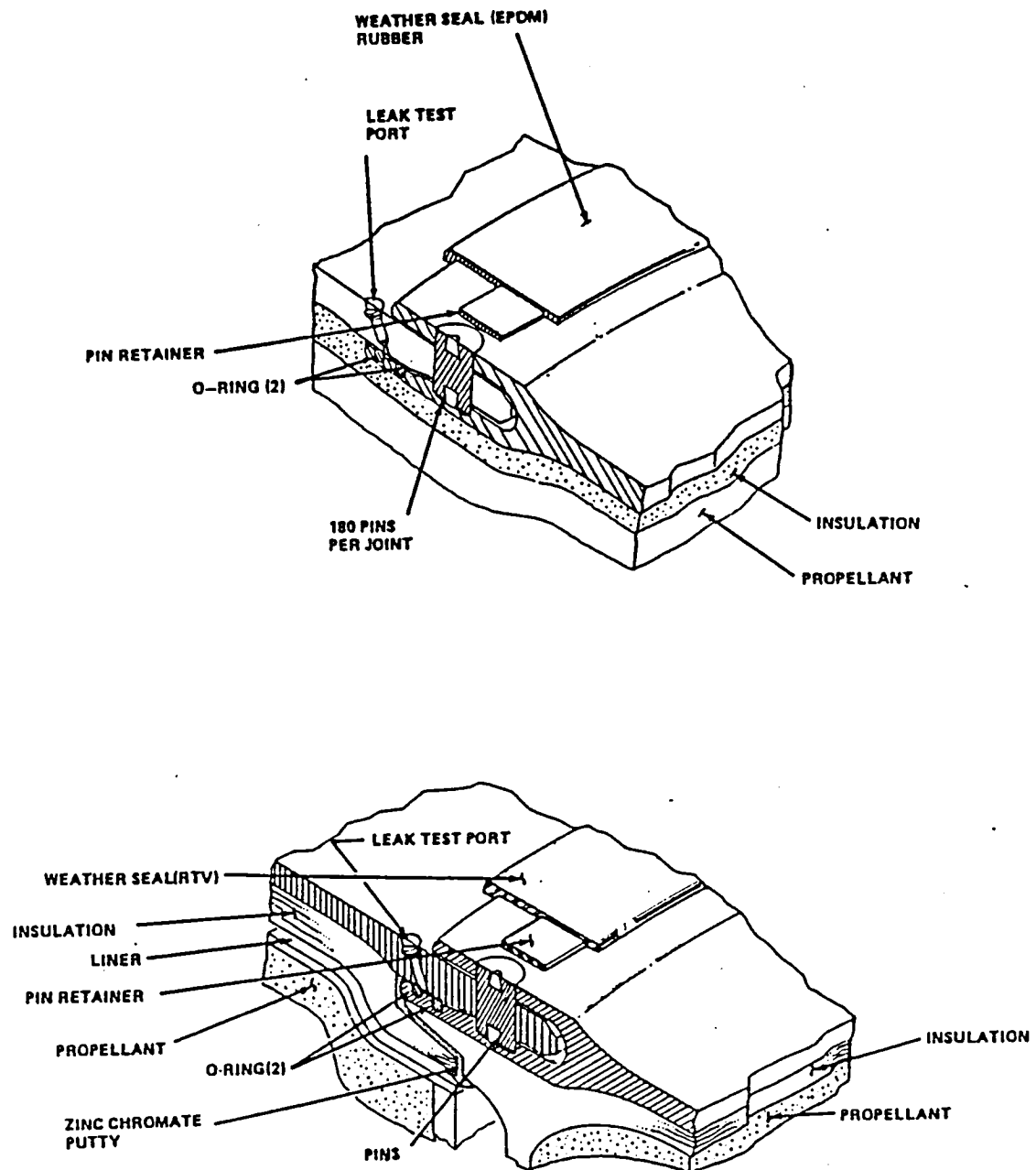
Fig. 20 SRM case joints.
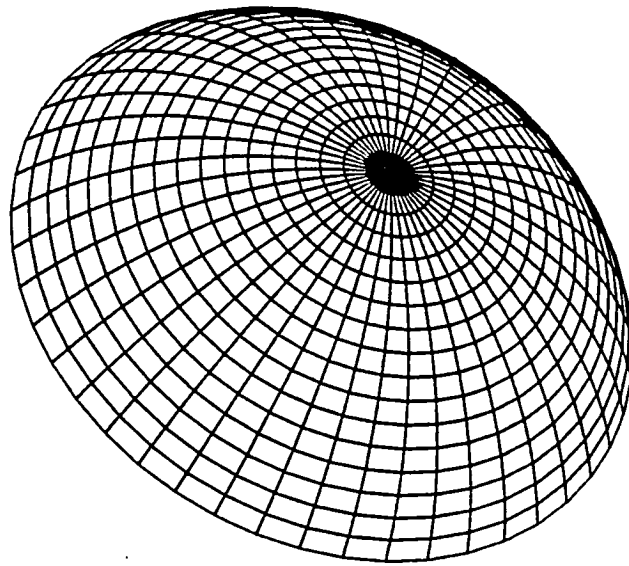
Fig. 21 Finite element model of forward dome.
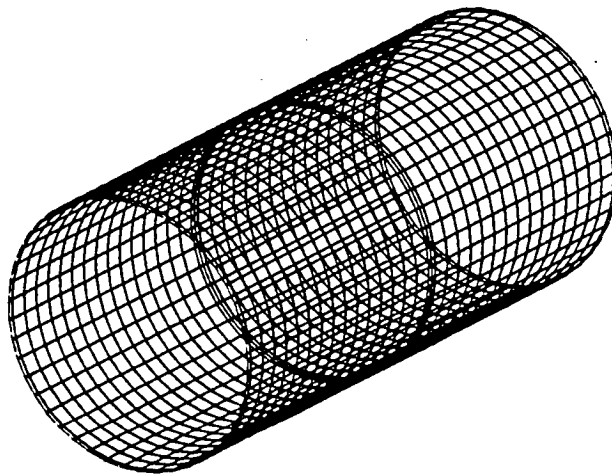
Fig. 22 Finite element model of forward cylinder case.
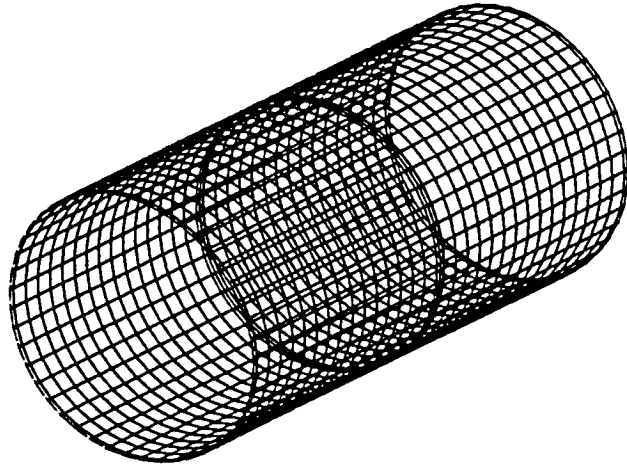
Fig. 23 Finite element model of forward center cylinder case.
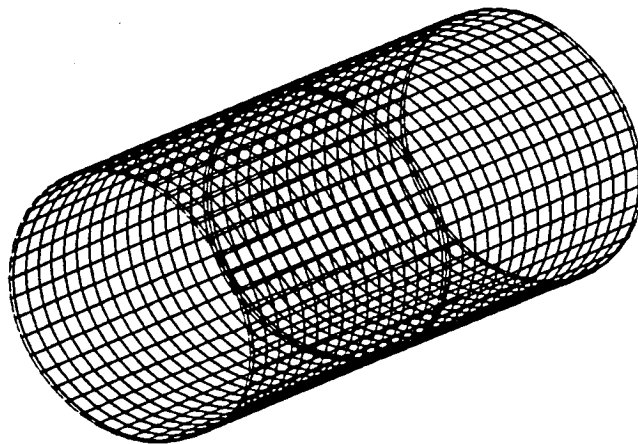
Fig. 24 Finite element model of aft center case.
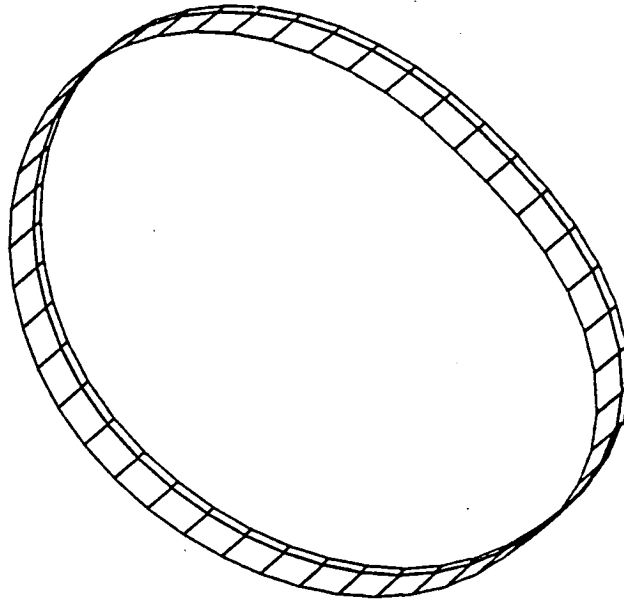
Fig. 25 Finite element model of aft attach case above SRM stub rings.
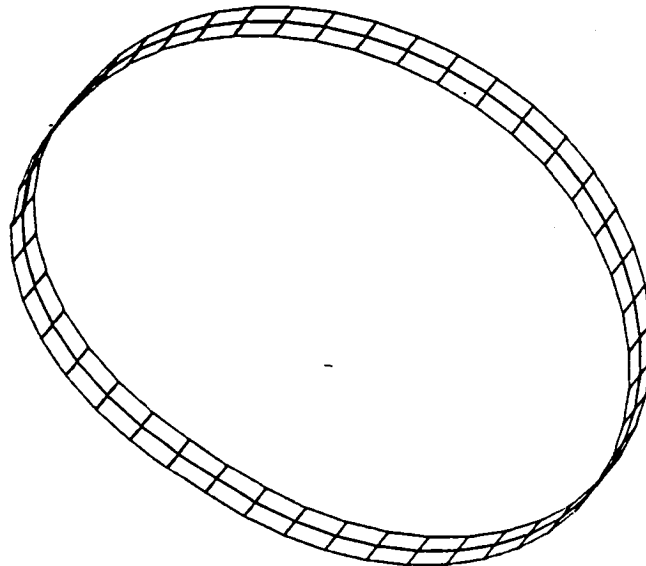
Fig. 26 Finite element model of aft attach case between SRM stub ring.
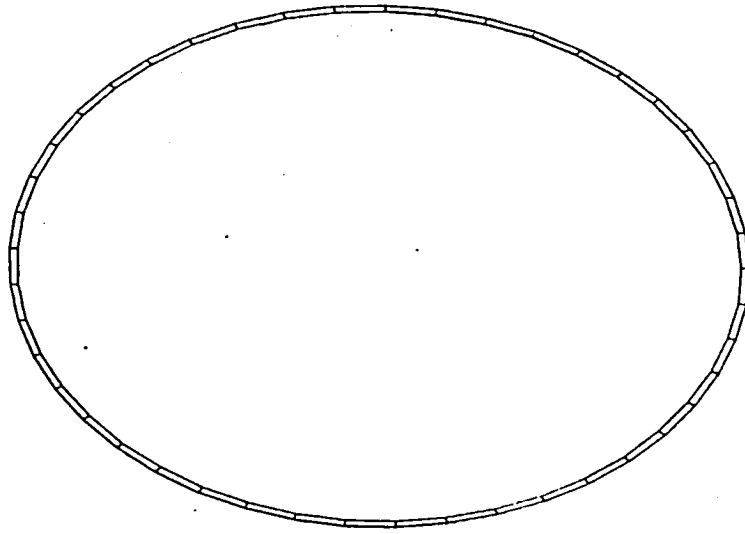
Fig. 27 Finite element model of SRM stub rings.
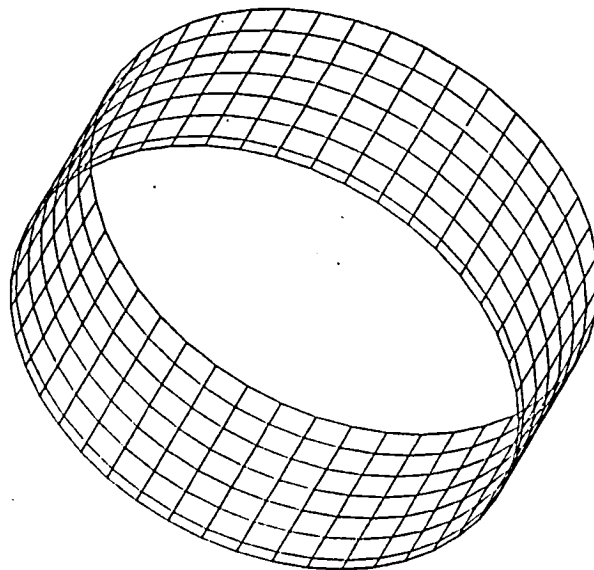
Fig. 28 Finite element model of aft attach case below SRM stub rings.
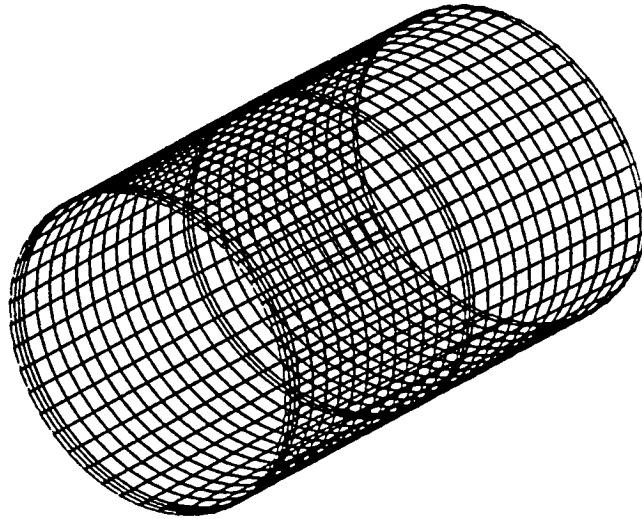
Fig. 29 Finite element model of aft attach case.
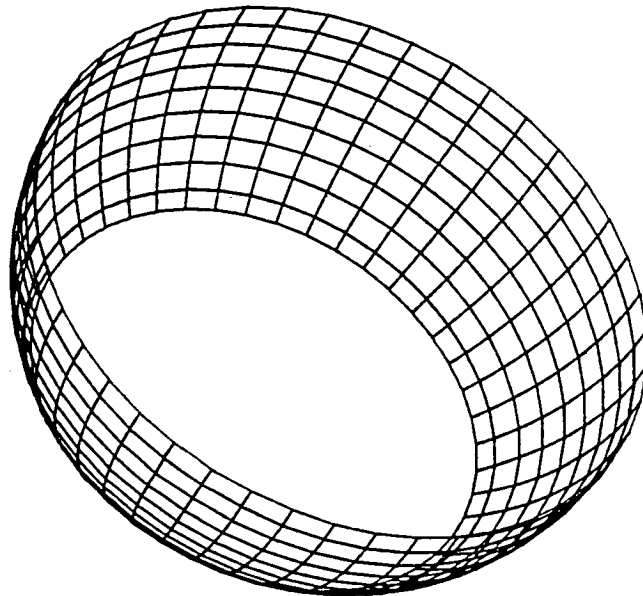
Fig. 30 Finite element model of aft dome.
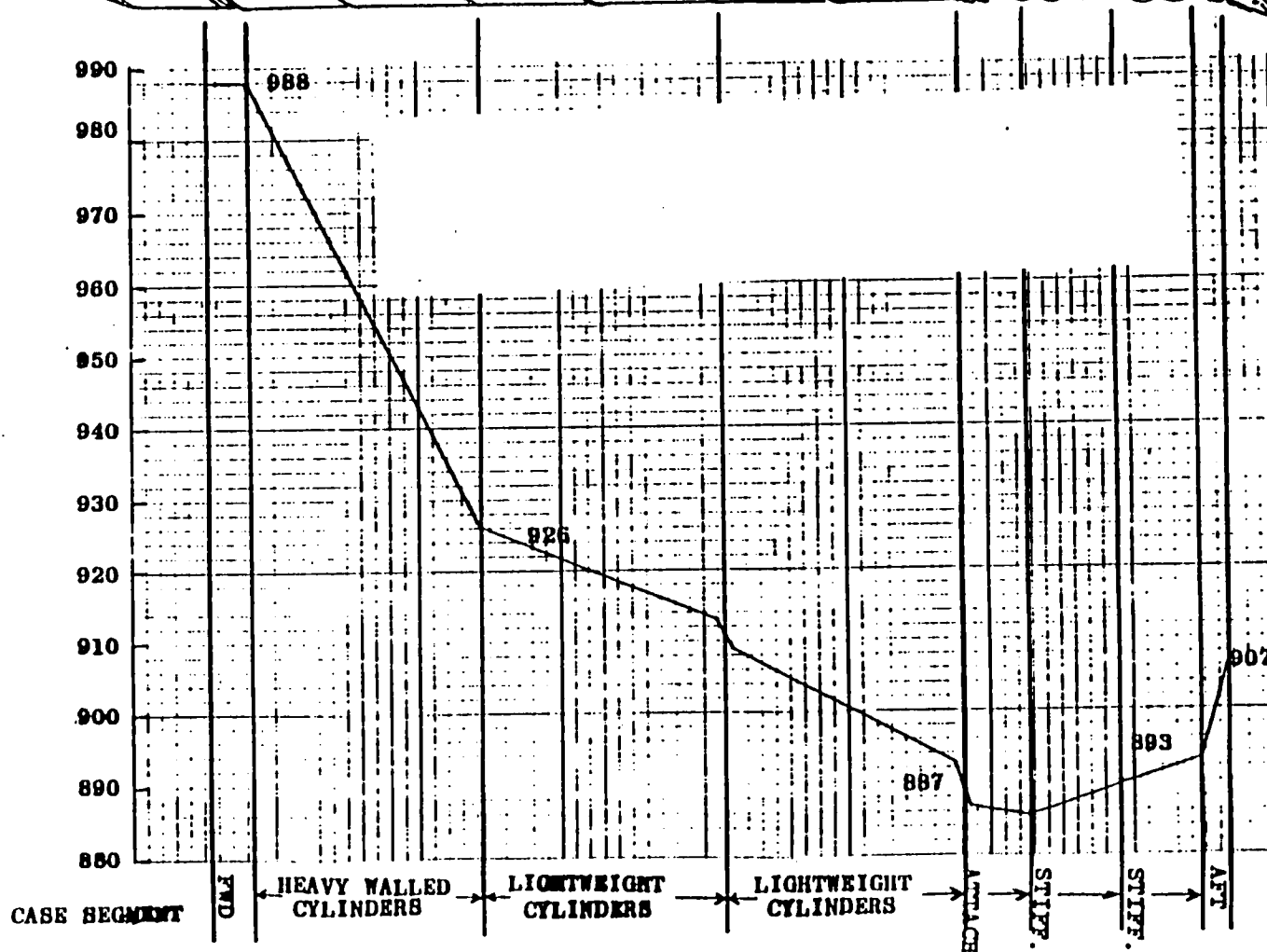
Fig. 31 SRM longitudinal pressure distribution (figure II-3 from reference 8).
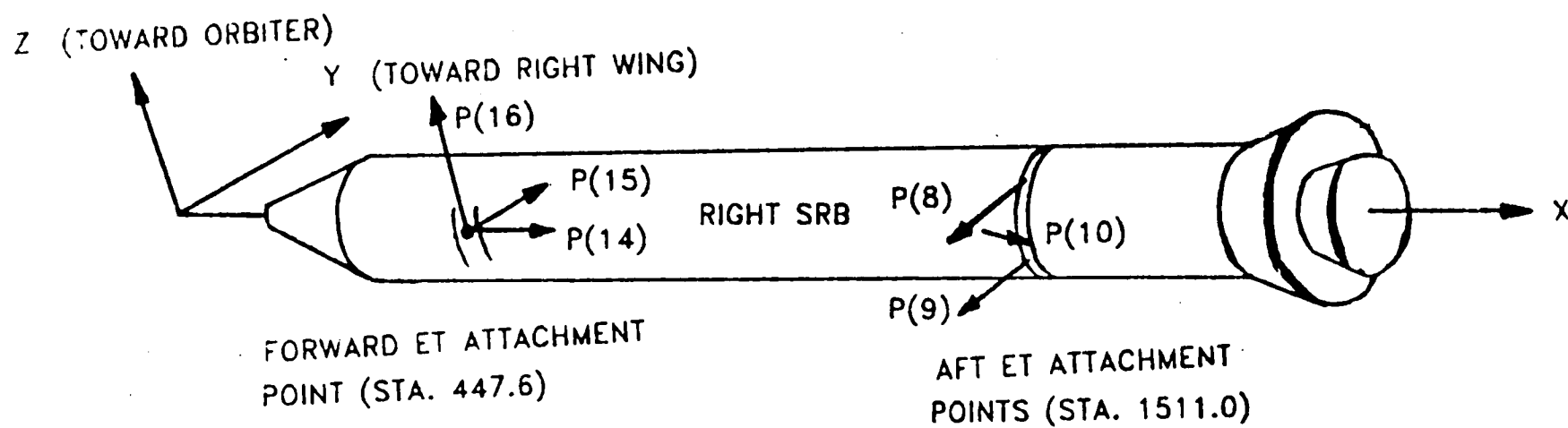
Fig. 32 SRB/ET interface loads.
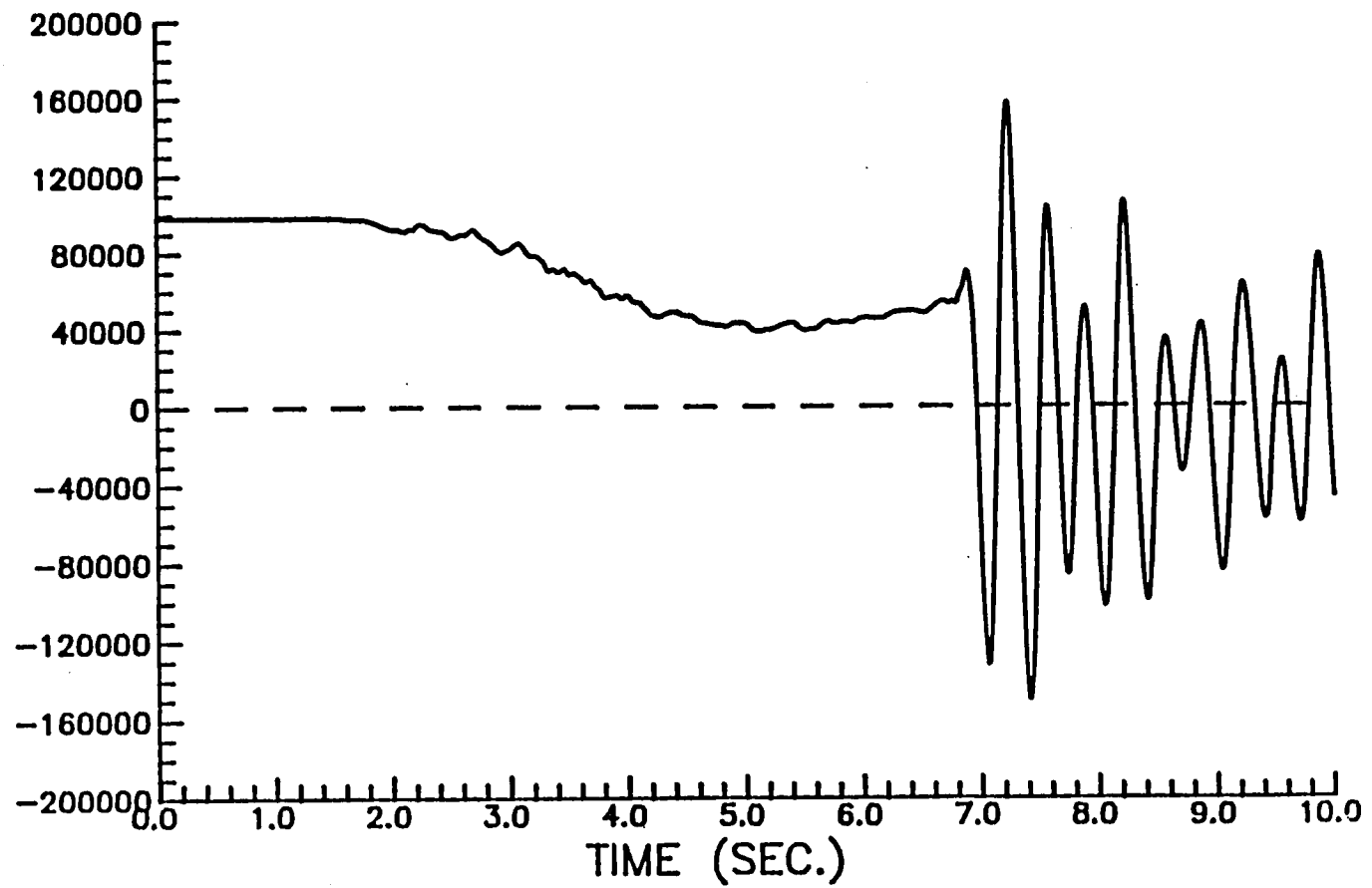
Fig. 33 Strut load P8 as a function of time.
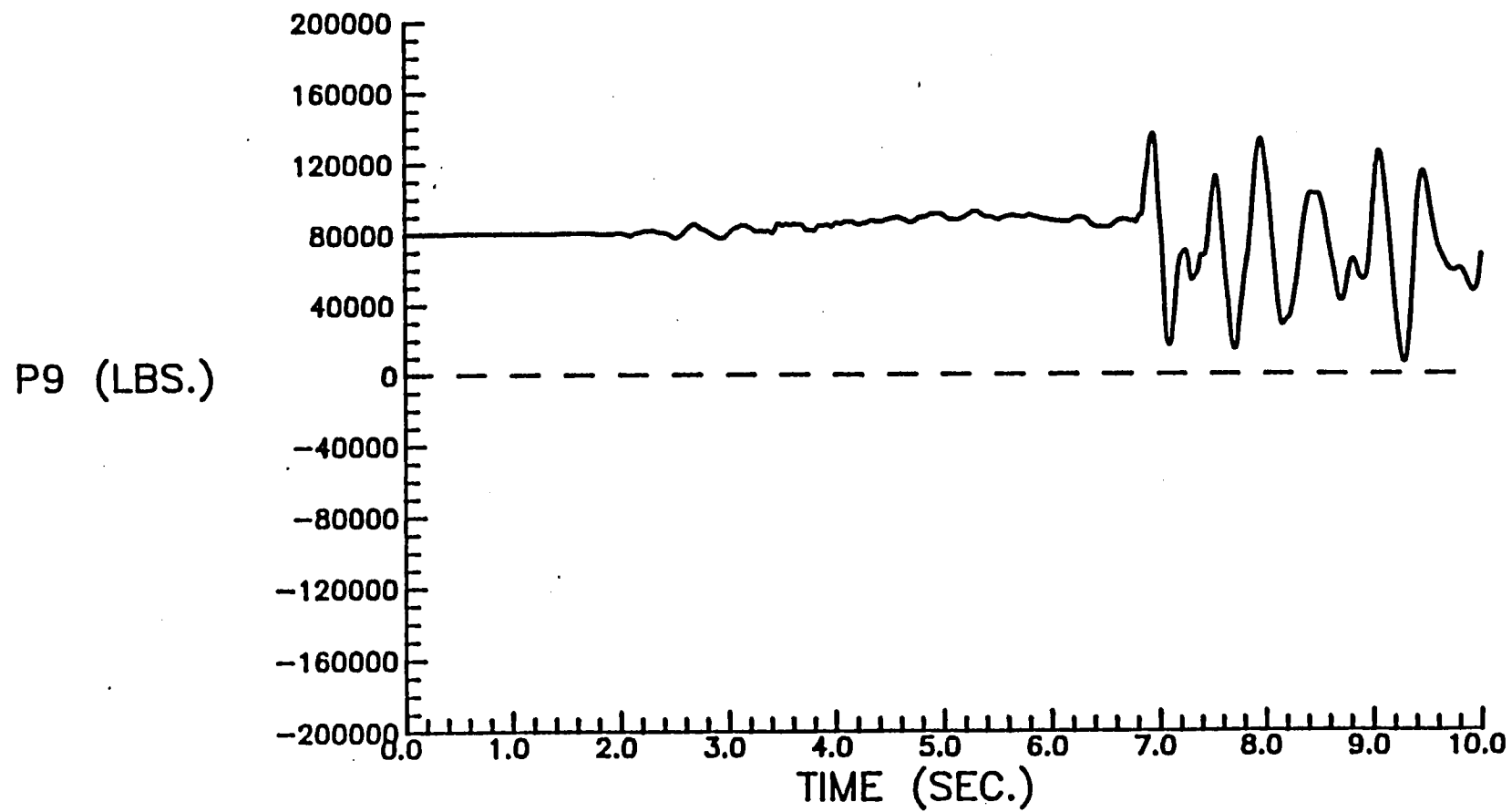
Fig. 34 Strut load P9 as a function of time.
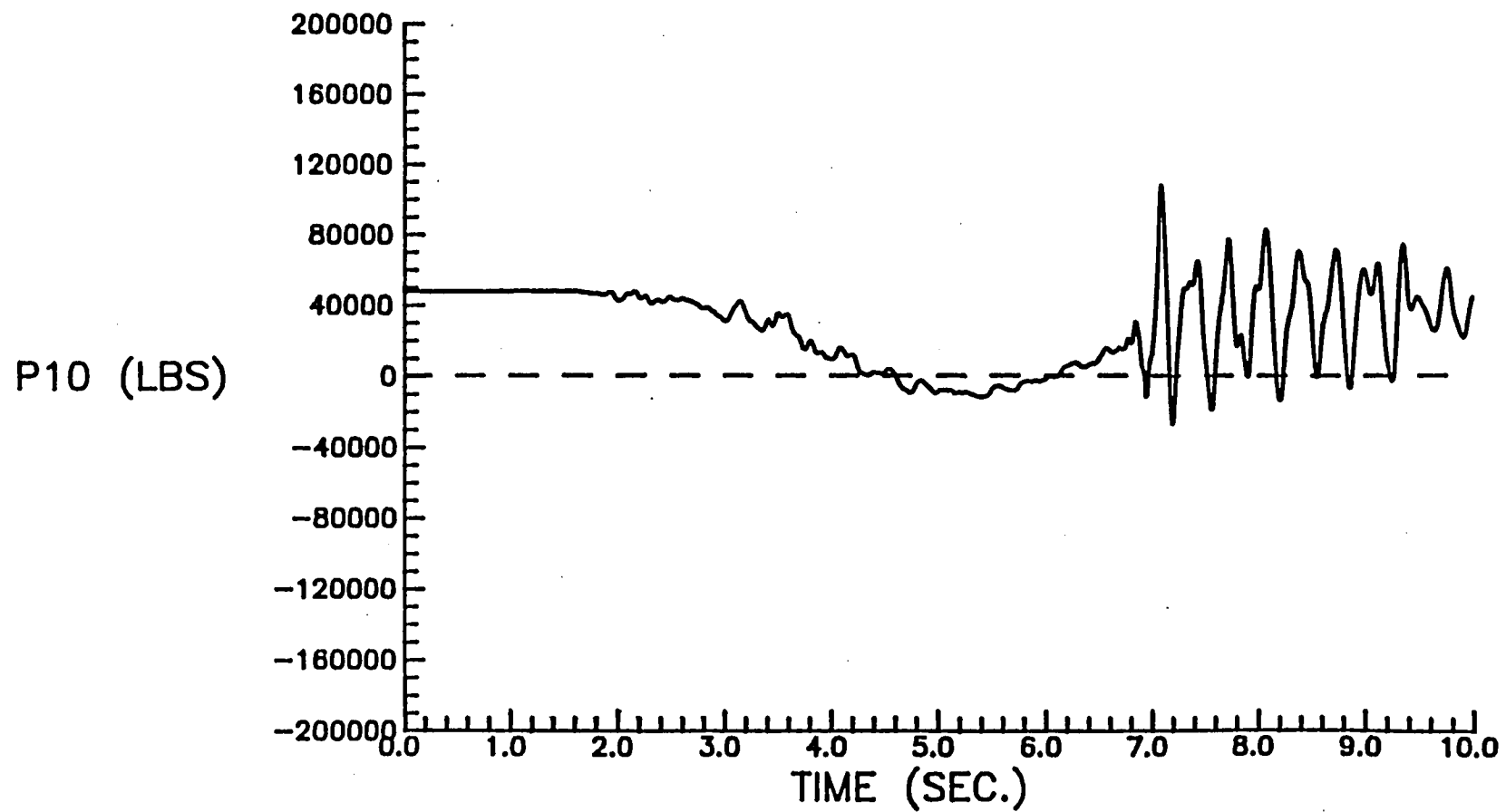
Fig. 35 Strut load P10 as a function of time.
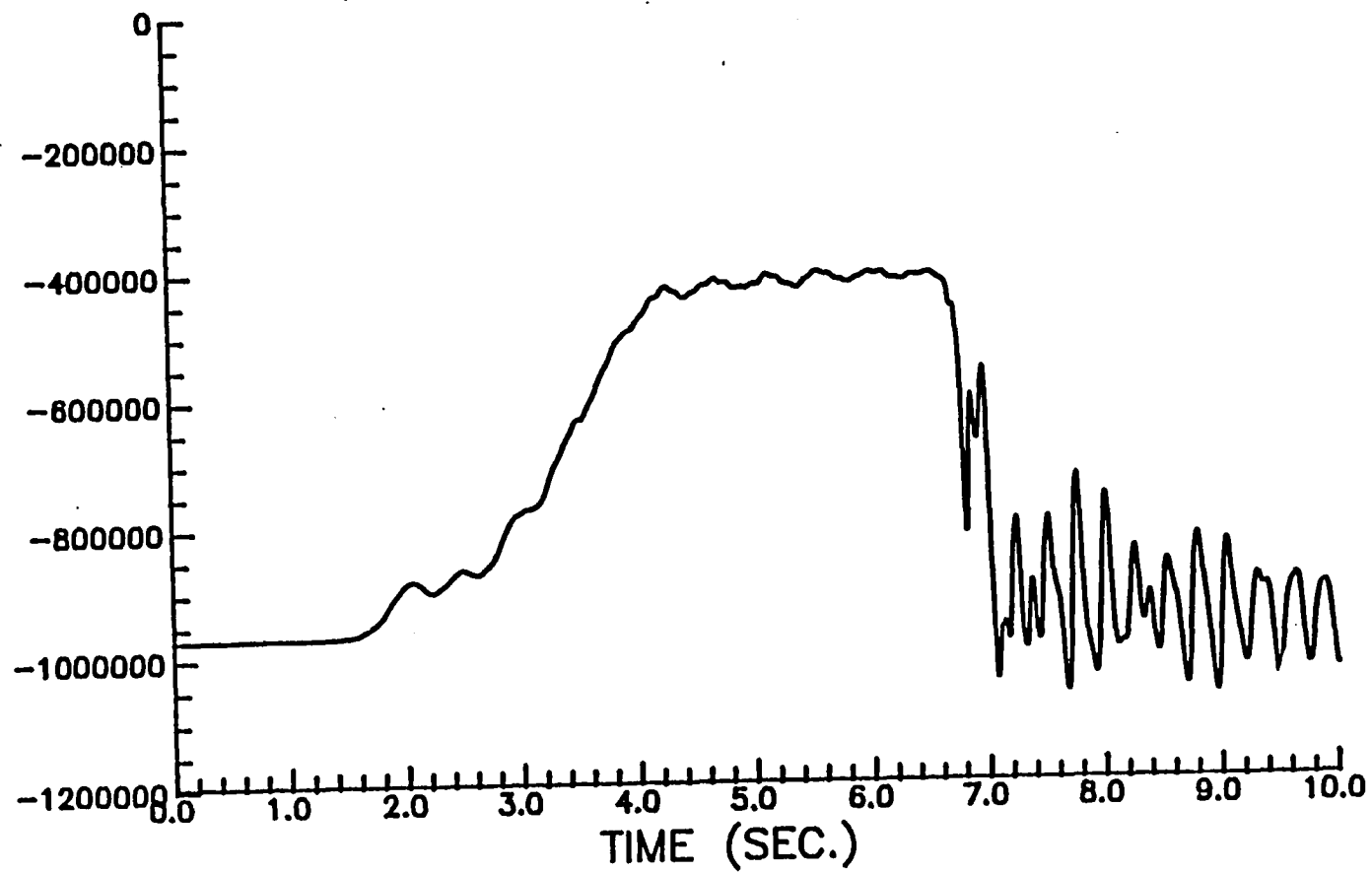
Fig. 36 Strut load P14 as a function of time.
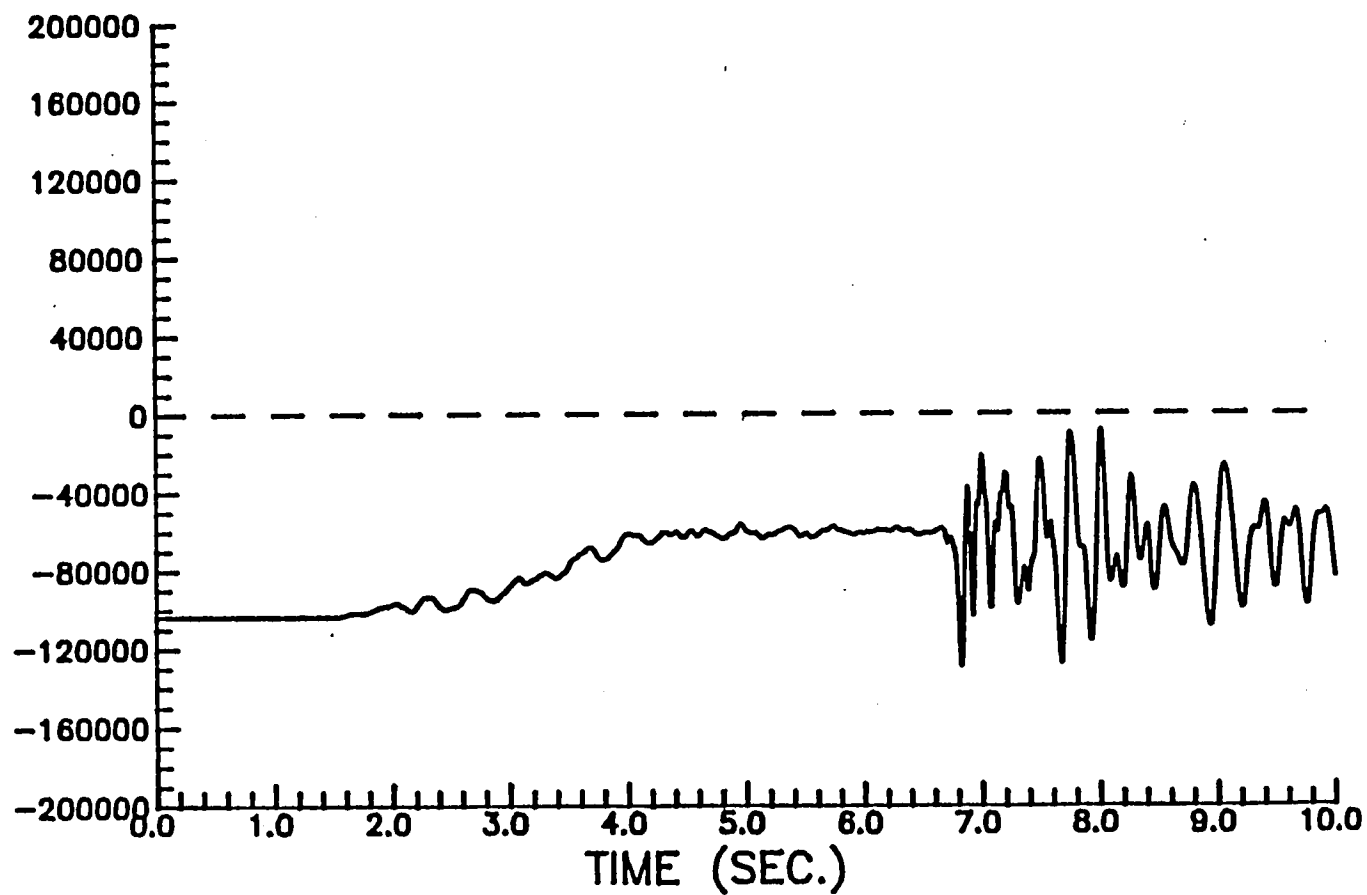
Fig. 37 Strut load P15 as a function of time.
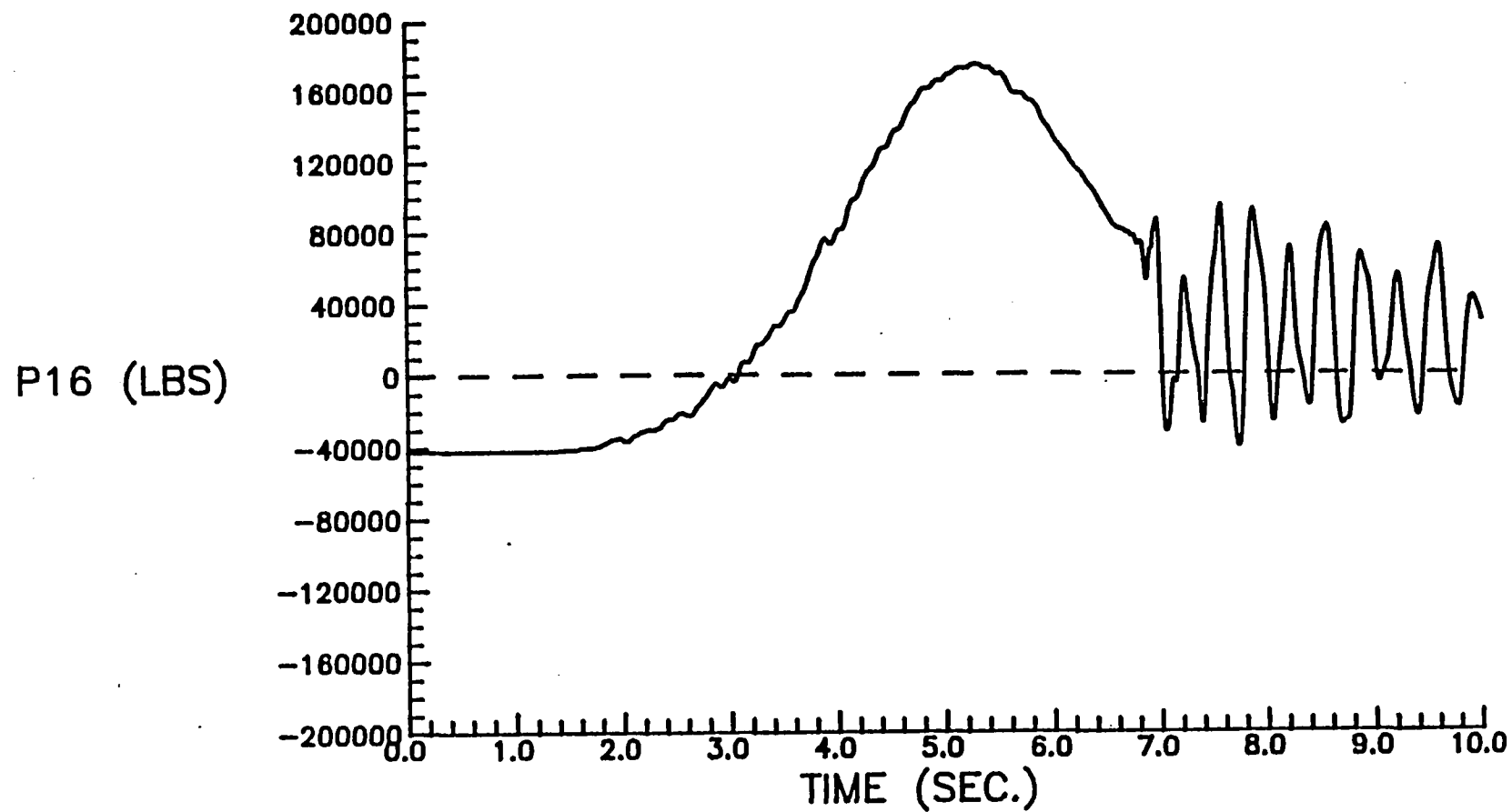
Fig. 38 Strut load P16 as a function of time.

Langley VAX 11/785

Model Preparation
and Verification,
Pre/Post-Processing
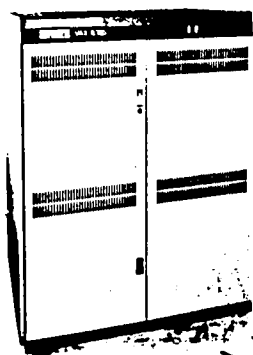
STAGS Data Sets (40Kbytes)

Ames NAS CRAY-2
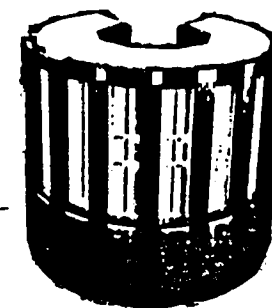
NASNET
(200Kbits/s)

STAGS Results (5 to 50Mbytes)

Number
Crunching

LARCNET
(256Kbits/s)

ACD

Plots, Printouts,
Microfiche

78

Fig. 39 Remote access to NAS computers.
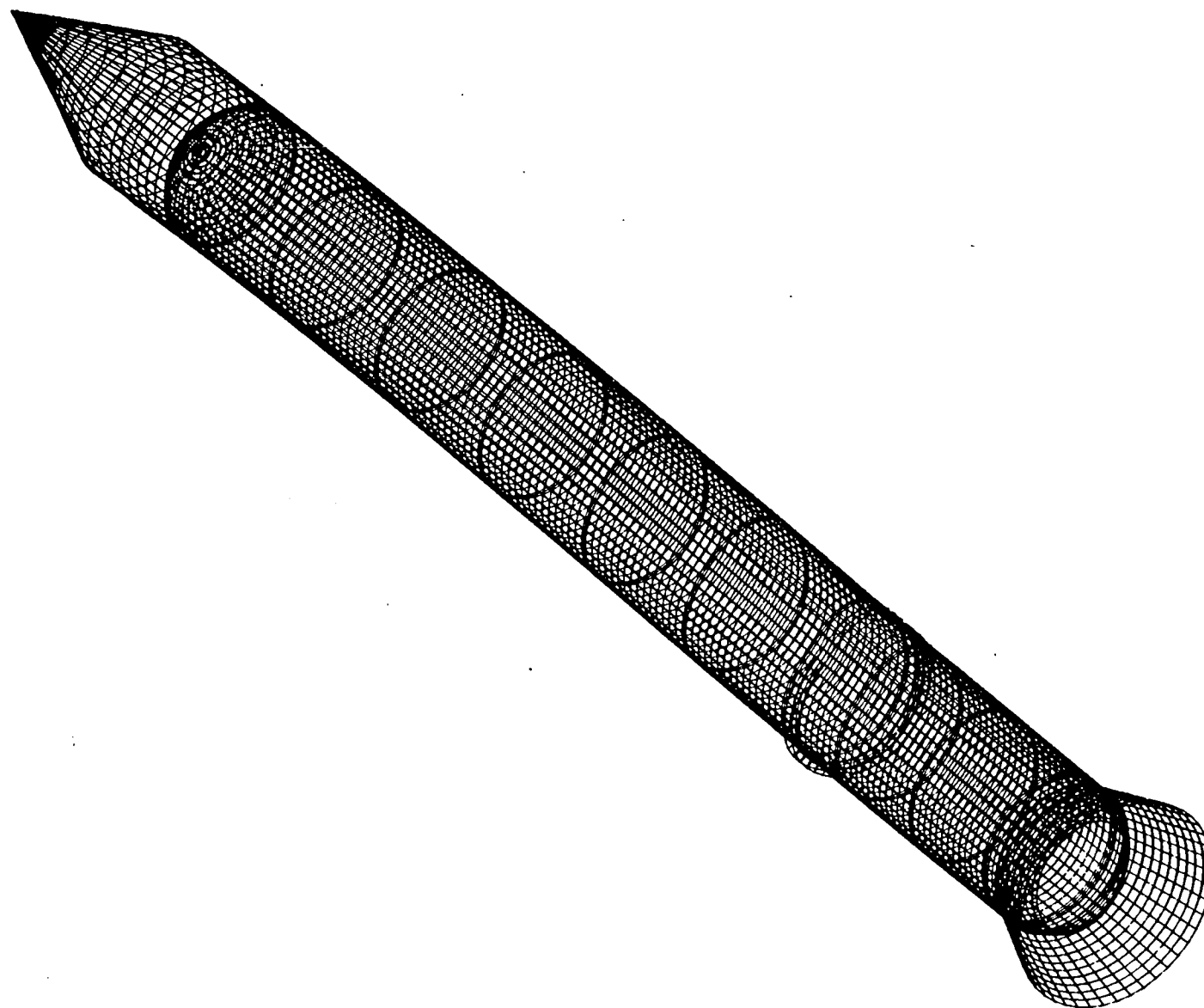
Fig. 40 Deformed geometry of the SRB corresponding to the time-consistent loads at t = 0
seconds (prior to SSME ignition).
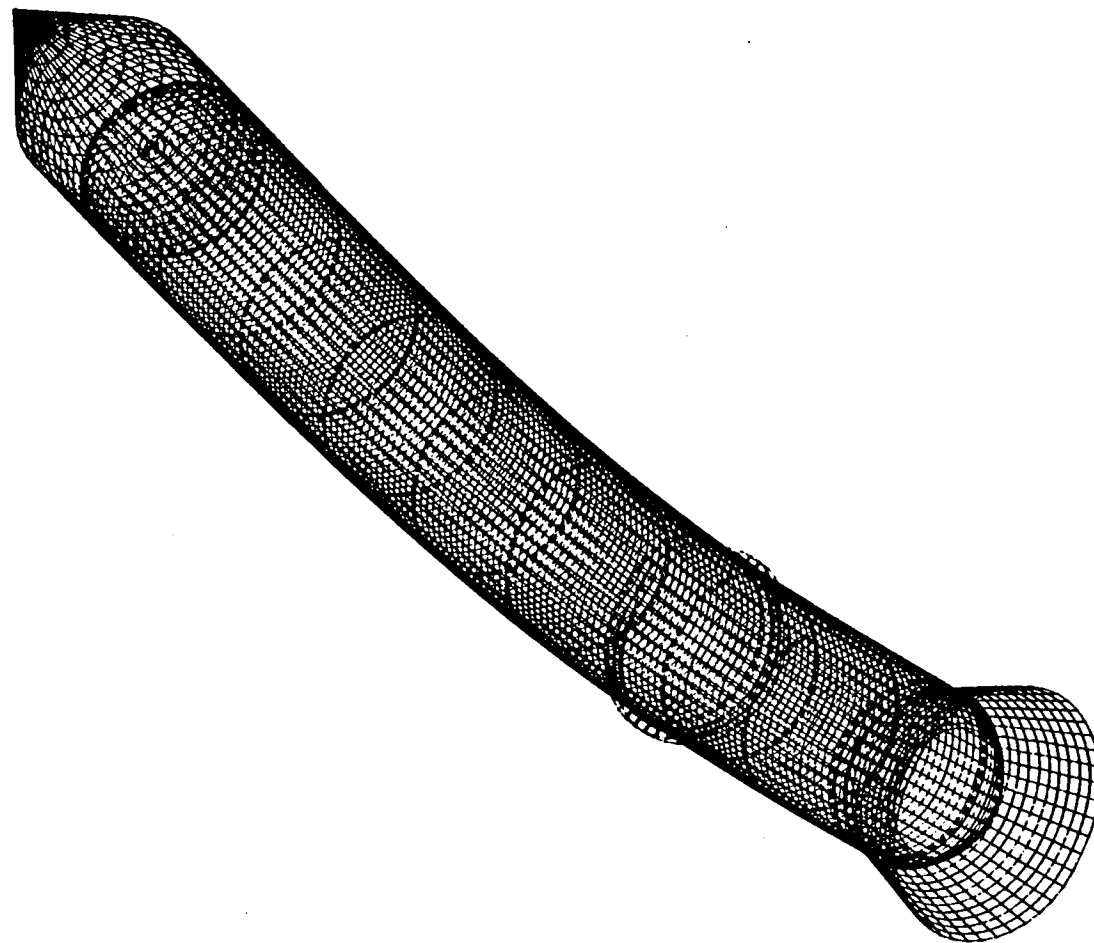
Fig. 41 Deformed geometry of the SRB corresponding to the time-consistent loads at t = 5.3 seconds ("max twang").
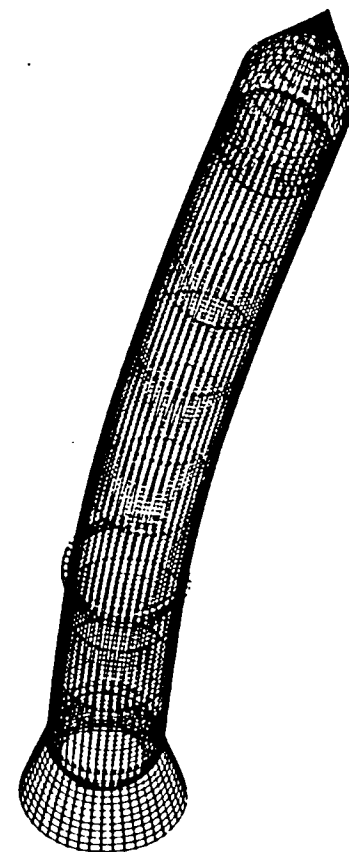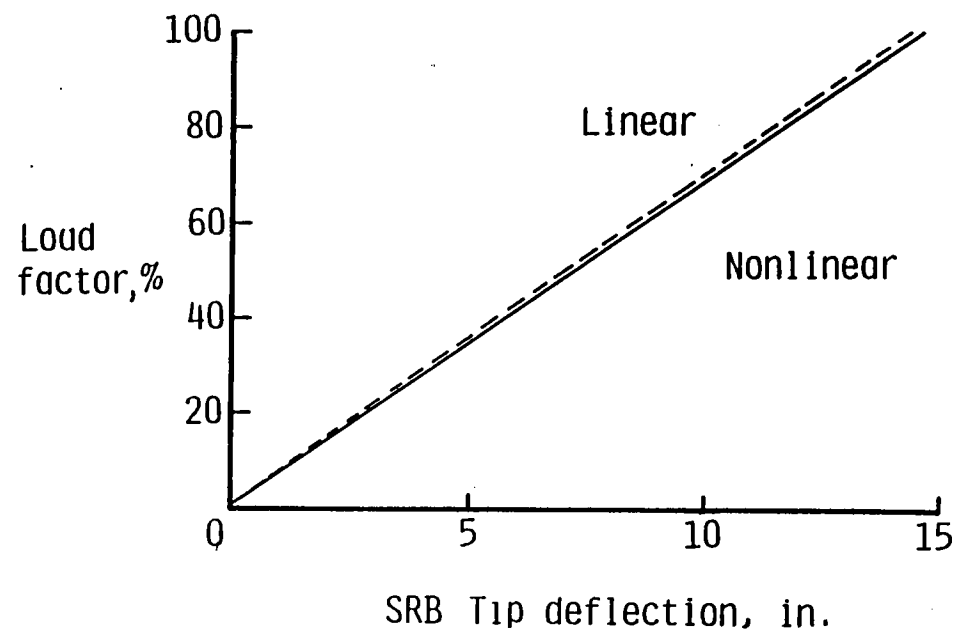
Fig. 42 Nonlinear response of the SRB tip using "max twang" loading.
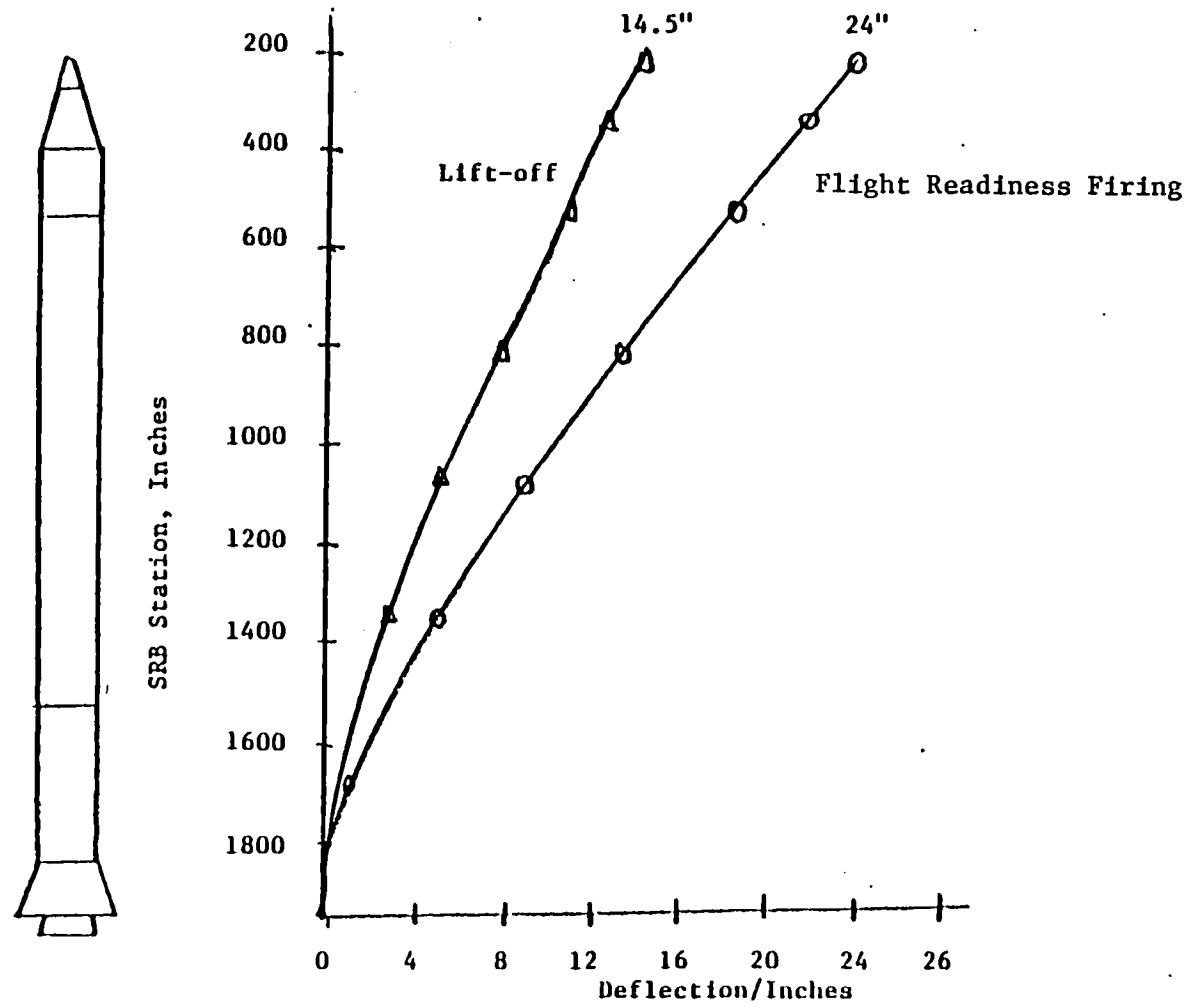
Fig. 43 SRB on-pad deflection distribution along its length.

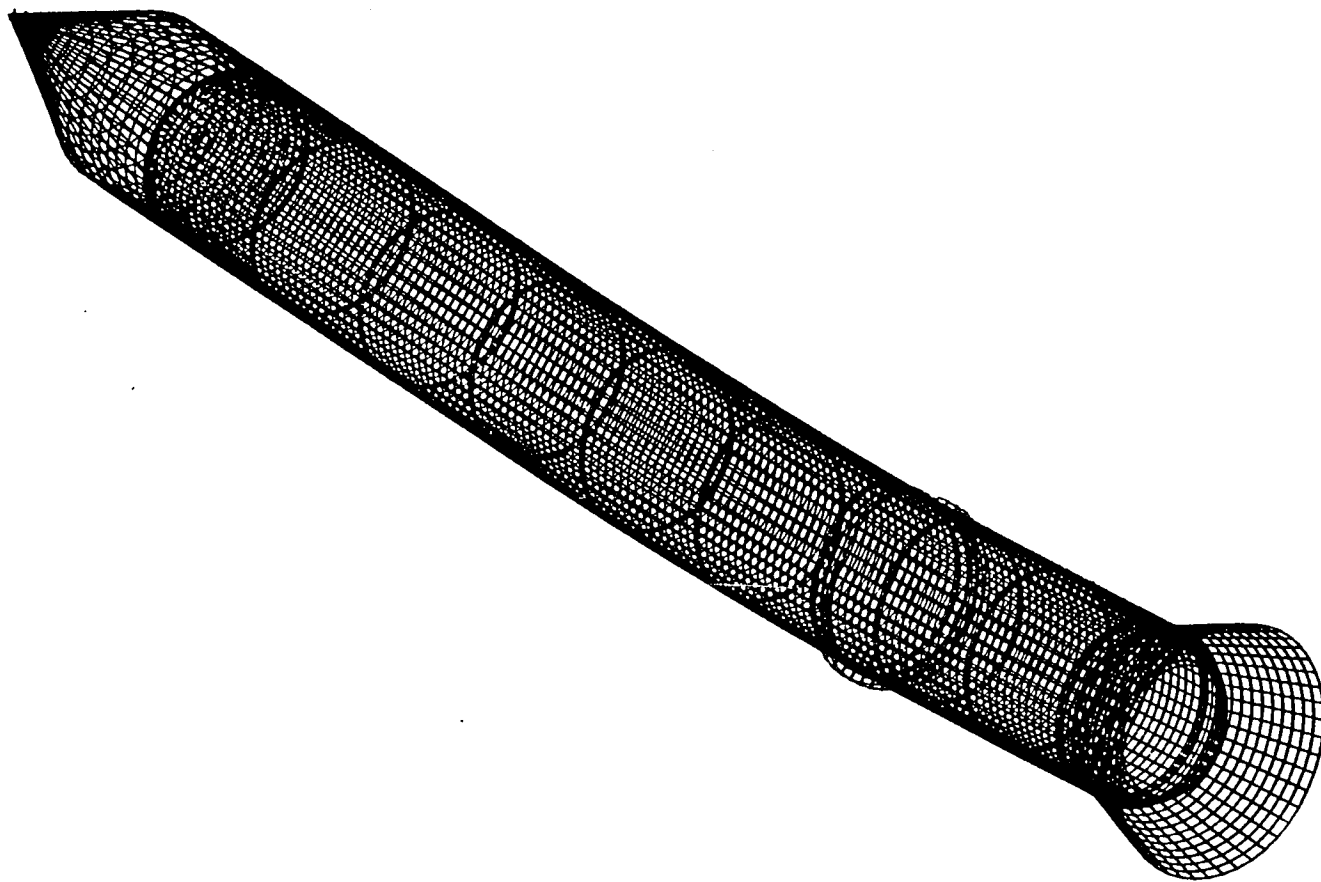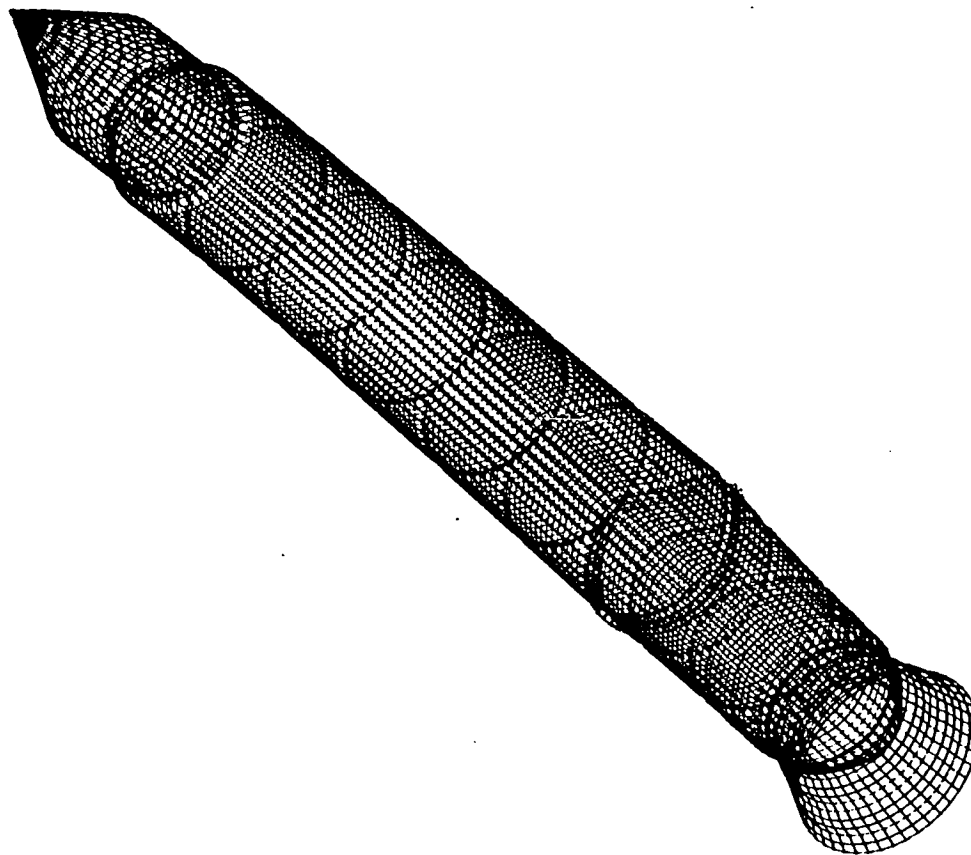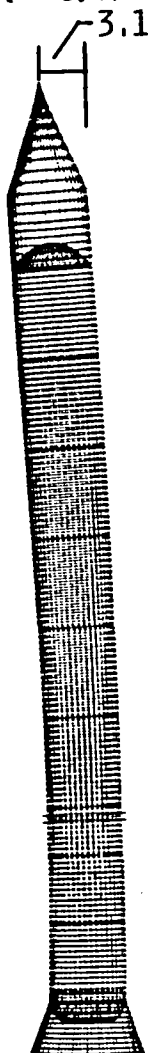Fig. 44 Deformed geometry of the SRB corresponding to the time-consistent loads at t = 6.6 seconds (SRM ignition).

Fig. 45 Deformed geometry of the SRB corresponding to the time-consistent loads at t = 7.2 seconds (prior to liftoff).
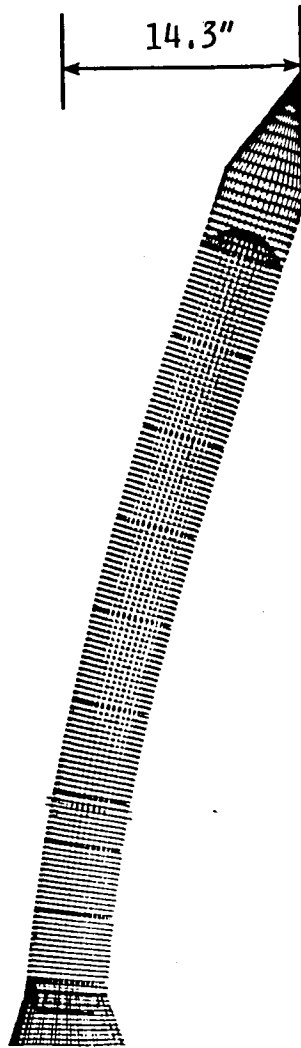
ET STRUT LOADS ONLY
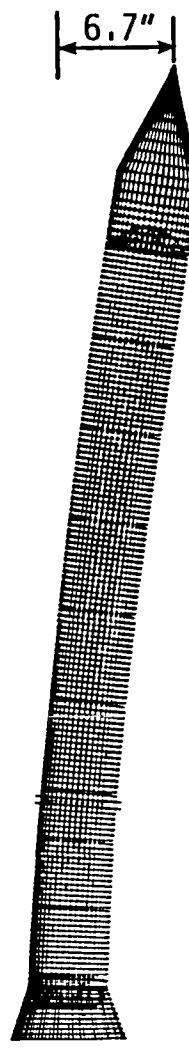
ET STRUT LOADS AND SRM PRESSURE

Prior to SSME ignition
(t = 0.0)

Max twang
(t = 5.3 sec)
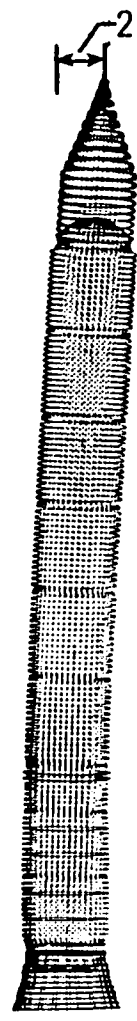
SRB ignition
(t = 6.6 sec)

Liftoff
(t = 7.2 sec)

3.1"

14.3"

6.7"

2.8"

Fig. 46 Summary of the deformed geometries of the SRB for the four time-consistent load cases considered.

NASA
National Aeronautics and Space Administration

Report Documentation Page

1. Report No. NASA TM-100515	2. Government Accession No.	3. Recipient's Catalog No.

4. Title and Subtitle		5. Report Date
Preliminary 2-D Shell Analysis of the Space Shuttle Solid Rocket Boosters		March 1988
		6. Performing Organization Code

7. Author(s)	8. Performing Organization Report No.
Norman F. Knight, Jr., Ronnie E. Gillian, and Michael P. Nemeth	

9. Performing Organization Name and Address	10. Work Unit No.
NASA Langley Research Center Hampton, VA 23665-5225	506-43-41-04
	11. Contract or Grant No.

12. Sponsoring Agency Name and Address	13. Type of Report and Period Covered
National Aeronautics and Space Administration Langley Research Center Hampton, VA 23665-5225	Technical Memorandum
	14. Sponsoring Agency Code

15. Supplementary Notes

16. Abstract

A two-dimensional shell model of an entire Solid Rocket Booster (SRB) has been developed using the STAGSC-1 computer code and preliminary 2-D shell analyses performed. The purpose of these analyses is to calculate the overall deflection distributions for the SRB when subjected to mechanical loads corresponding to critical times during the launch sequence. The mechanical loading conditions for the full SRB arise from the External Tank (ET) attachment points, the SRM pressure load, and the SRB hold down posts. The ET strut loads vary with time after the Space Shuttle Main Engine (SSME) ignition. The Solid Rocket Motor (SRM) internal pressure varies axially by approximately 100 psi. Static analyses of the full SRB are performed using a "snapshot picture" of the loads.

The SRB analyses are performed using various NASA computer systems. In building the finite element models, calculating results, and evaluating the output, three different classes of computer systems are used (i.e., workstations, minicomputers and supercomputers). A fourth class of computer system, the mainframe system, is used to store data, process microfiche, and produce report-quality graphics output. The computational approach using this variety of computer systems is described.

17. Key Words (Suggested by Authors(s))	18. Distribution Statement
Solid Rocket Boosters Space Shuttle Structural Analysis STAGS	Unclassified—Unlimited Subject Category 39

19. Security Classif.(of this report)	20. Security Classif.(of this page)	21. No. of Pages	22. Price
Unclassified	Unclassified	90	A05

NASA FORM 1626 OCT 86